Computer Assisted Methods in Engineering and Science, **25**: 89–120, 2018, doi: 10.24423/cames.246

TWENTY-FIVE YEARS OF THE CAMES

Simulation of dynamic phenomena in a high pressure variable displacement axial piston hydraulic pump

Tomasz Zawistowski[1], Michał Kleiber[2]
[1] *Creotech Instruments S.A.*
Okulickiego 7/9, 05-500 Piaseczno, Poland
e-mail: tomasz.zawistowski@creotech.pl
[2] *Institute of Fundamental Technological Research*
Polish Academy of Sciences
Pawińskiego 5b, 02-106 Warsaw, Poland
e-mail: mkleiber@ippt.pan.pl

Substituting a valve plate-based commutation unit with a hydrostatic-load-free commutation bushing controllable with a signal of negligible power, that could be applied in constant and variable displacement pumps introduced a different approach to the design of commutation units in multi-piston axial hydraulic pumps.

Conducted research showed that valve plate-based commutator is responsible for over 50% energy loss. The new idea assumed a stationary cylinder block and the replacement of the valve plate with a cam-driven commutation unit that would be totally unloaded hydrostatically. That eliminated main source of mechanical losses as well as a flow resistance loss. Additionally, the dead volume was significantly reduced, which helped to reduce the pump noise level and resulted in a great decrease in power needed to control the pump displacement. That allowed to eliminate a servomechanism and the direct control of the pump displacement with a low power element. However, the new design presented a challenge in the form of pressure peaks occurring in the working chamber, which were difficult to eliminate. This article presents attempts to solve problems connected with those dynamic phenomena.

Keywords: hydrostatic machine, axial multi-piston pump, dynamic phenomena.

1. INTRODUCTION

The design of the PWK pump was developed in the Department of Hydraulics and Pneumatics of the Gdańsk University of Technology and is covered by international patents [4, 5, 7, 8].

A detailed cross section of the PWK pump is shown in Fig. 1 It presents the topology of the pump which was the baseline of a new concept describing the cam-driven commutation unit. There are two swash plates (2) mounted on a drive shaft (1). Cylinder block (3) is immobilized in the pump case. Two pistons (4) are moving in opposite directions and are connected by means of piston shoes (5) to swash plates (2). The commutation unit comprises a bushing (6) and follower fingers sliding in a cam grove (7). The cam can slide on a drive shaft (1) driven by the electromagnet (8) and a pushing rod (9). When the cam (7) is in the left-most position (as shown in Fig. 1), then the working chamber is connected to the low and high pressure orifices, the same amount of time and the capacity setting of the pump is maximum. Shifting the cam to the right shortens the connection time between the working chamber and the high pressure port, while the connection time with the low pressure port increases which lowers the efficiency of the pump. In the right-most position of the cam (7) the working chamber is constantly connected to the low pressure port thus bringing the pump capacity to zero.

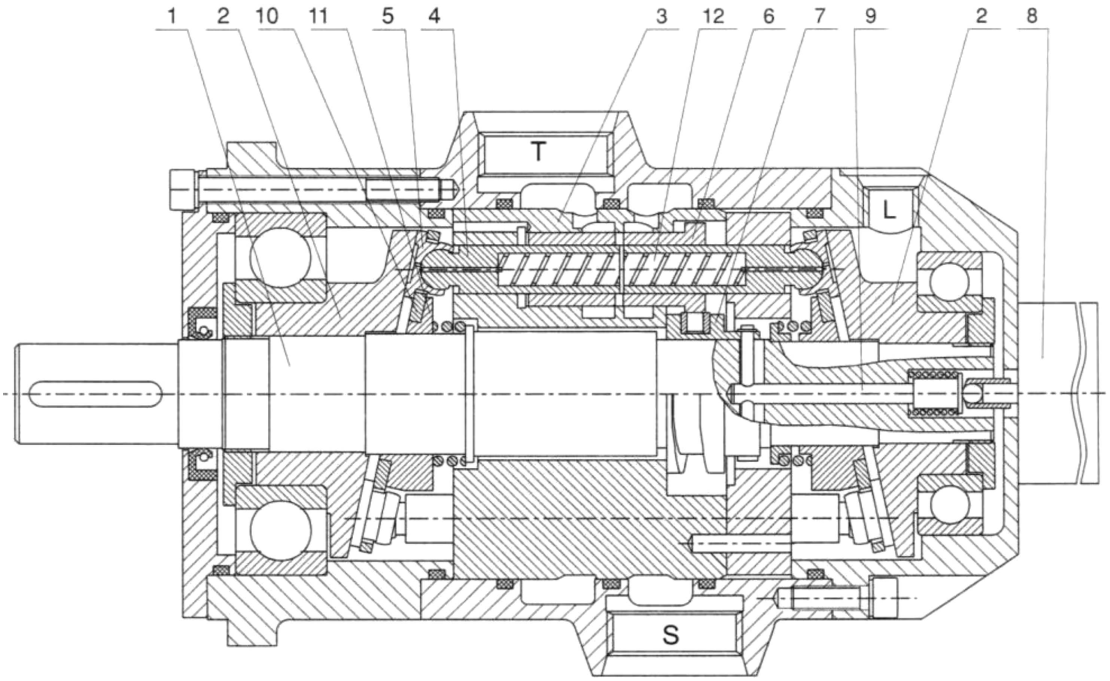

Fig. 1. A detailed cross section of the PWK pump (credit: [2]).

A simplified view of the PWK-type pump rendering is shown in Fig. 2.

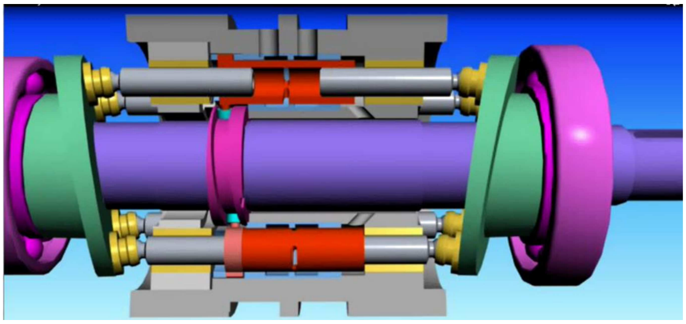

Fig. 2. Animated view of the PWK pump (credit: [6]).

2. Cam-driven capacity control

Variable capacity control of the PWK pump was described in [2]. The cam rotates by means of the planetary gear driven by the stepper motor. Hydrostatic machines using that method of setting capacity provide advantages compared to the traditional, widely used pumps while maintaining the most valuable properties of those pumps. The capacity controlling mechanism is independent of the direction of rotation of the pump as well as the pressure in the high pressure port.

Here are characteristics of the cam-driven commutation unit:

- individual cylindrical commutation sleeve driven by the centrally-located cam. It allows the total unloading of the hydrostatic load, eliminates the source of the biggest energy losses and increases reliability;
- almost a full contact of opposite piston faces at the end of the pressure cycle. With additional helical throttles inserted into pistons and small volume of inlet windows in commutating bushings

the dead volume was decreased from 20 up to 40 times compared to the machines with valve port commutation units;

- fixing the swash plate inclination angle and changing the pump capacity control method eliminated not only energy losses (in traditional pumps could cause capacity decrease of 30% and more) but also eliminated the source of noise caused by rapid compression and decompression of fluid in the dead volume;
- a new way of controlling the pump capacity by moving a cam along the drive shaft is characterized by small forces needed to reposition the cam. That could be realized by an electromagnet or a stepping motor, thus eliminating a hydraulic servomechanism and reducing the pump size and mass;
- immobilizing a cylinder block reduces pressure losses in ports and improves the cavitational characteristics of the pump which can work as a self-sucking device.

Compared to a traditional valve plate commutation axial pump the PWK pump presents features shown in Table 1.

Table 1. Comparison of PWK characteristics with a traditional axial pumpdesign.

Traditional axial pump	PWK axial pistion pump
Type of commutation unit	
Valve plate	Cam-driven
Kinematics of the cylinder block	
Block rotates with the drive shaft	Block is stationary
Characteristics of the dead volume	
Can exceed 100 % of working volume	Reduced dead volume; independent of displacement setting
Oil throttling	
Insufficient throttling of oil	Use of helical throttles
Capacity control	
Displacement change by varying the angle of swash plates	Cam mechanism controls variable displacement

3. CAM-CONTROLLED COMMUTATION UNIT AND ITS CHALLENGES

The major elements of a particular working chamber (there are 7 working chambers along the perimeter of the cylinder block) are presented in Fig. 3. A commutation bushing is moving freely in the cylinder block between low and high pressure ports. Pistons which move in the opposite directions in a commutation bushing are driven by swash plates, while the bushing is controlled by the drive-shaft-mounted cam with which a follower finger provides a contact. When the bushing moves to the left and connects the working chamber with the low pressure port – pistons within the bushing are forced to move outwards – sucking the hydraulic fluid into the working chamber. When the chamber is filled with oil, the commutation bushing moves in the opposite direction and connects the working chamber with the high pressure port. At that point pistons start to move inwards displacing the fluid from the working chamber into the high pressure port. That process lasts till the commutation bushing returns to its neutral position, where the commutation window is blocked off by the bridge between two pressure ports trapping the fluid which is being compressed by moving pistons. That results in an instantaneous increase of oil pressure in the working chamber in variable displacement pumps, although it is only observable at displacements different from 100%. The PWK pump designers strived to eliminate such phenomenon. This paper addresses methods that were applied in attempts to eliminate rapid increase of pressure in the working chamber at the moment where the working chamber was blocked off from pressure ports by the bridge separating the ports (see Fig. 3). There are several ways that could help eliminate such pressure peaks, like the evacuation of excess of oil from the working chamber or the reduction of time when the working chamber is cut off from either of pressure ports.

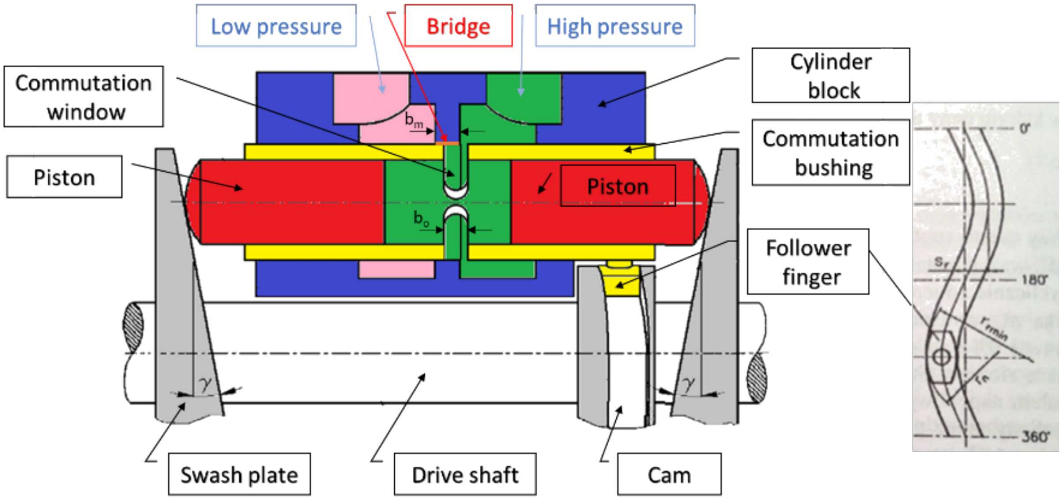

Fig. 3. General schematic of one of 7 working chambers of the PWK pump with the unfolding view of a cam (credit: [6]).

4. METHODOLOGY OF FINDING A SOLUTION

The problem solving process focused on identifying factors possibly responsible for the occurrence of pressure peaks in the working chamber. The value of pressure peaks in the working chamber could be influenced by factors like:

- average pumping pressure;
- oil bulk modulus;
- volume of fluid in the chamber;
- leakage;
- temperature;
- displacement adjustment;
- rotational speed;
- deformation of pump elements.

In the presented methodology only the pump construction design-related issues were described. When those causes were established, the methods of simulating respective phenomena were defined and the process of result validation was set up. The general methodology structure is presented in Fig. 4.

In the first place the CAD model of the pump was created. Its rendition is presented in Fig. 5.

Subsequently a CFD model of the pump was defined starting with a simple 2D approximation.

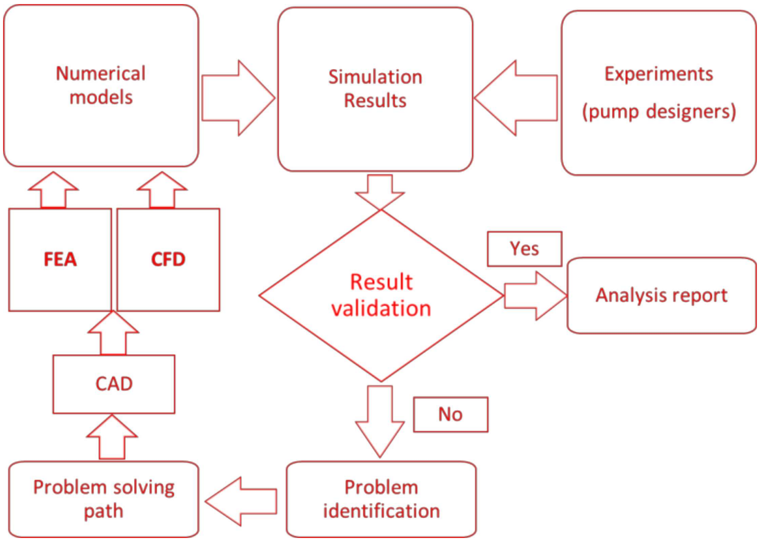

Fig. 4. Methodology of the problem solving process.

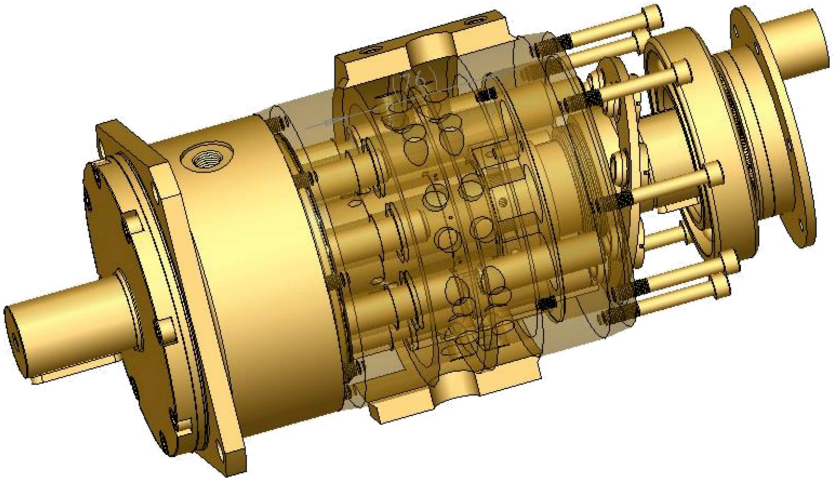

Fig. 5. CAD model of the PWK pump.

5. CFD MODEL DESCRIPTION

The model of fluid flow described in [1] was based on the following assumptions: a coupled pressure-based-solver, Spallart-Almaras turbulence model, transient fluid flow. The harmonic motion of pistons was described by

$$v = A\omega \sin(\omega t), \tag{1}$$

where v – velocity either of the commutation bushing (at 1000 rpm the speed of the bushing was 0.52 m/s) or pistons (whose maximum speed would be 1.3 m/s), A – amplitude of a half stroke (for the bushing equal to 5 mm, for the pistons = 12.59 mm), ω – angular velocity (for 1000 rpm equal to 104.72 rad/s), t – time.

To start with a simple 2D axisymmetric model of the fluid one cylinder was set up with a low pressure port which was fixed while the commutating bushing window and the working chamber were moving. A commutating window was moving in a harmonic motion and the working chamber was modelled with a dynamic mesh, which was expanding and contracting during the cycle.

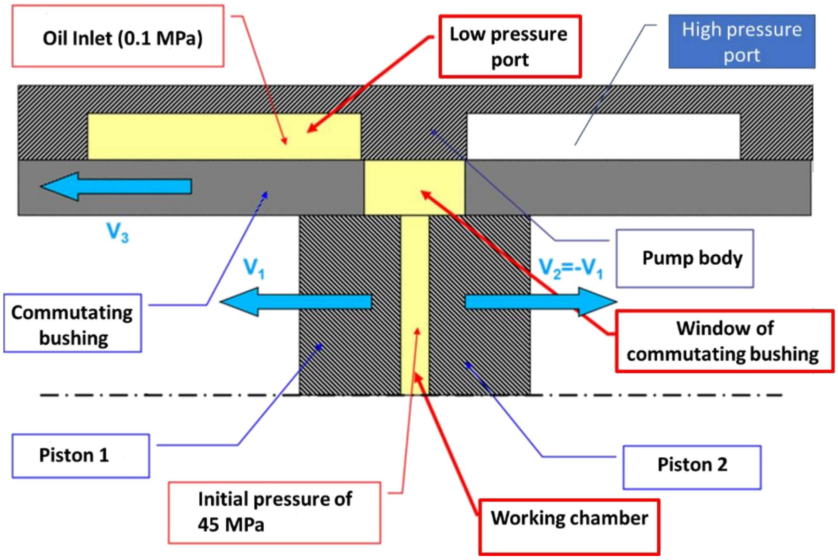

Fig. 6. Simplified 2D model components during the cycle.

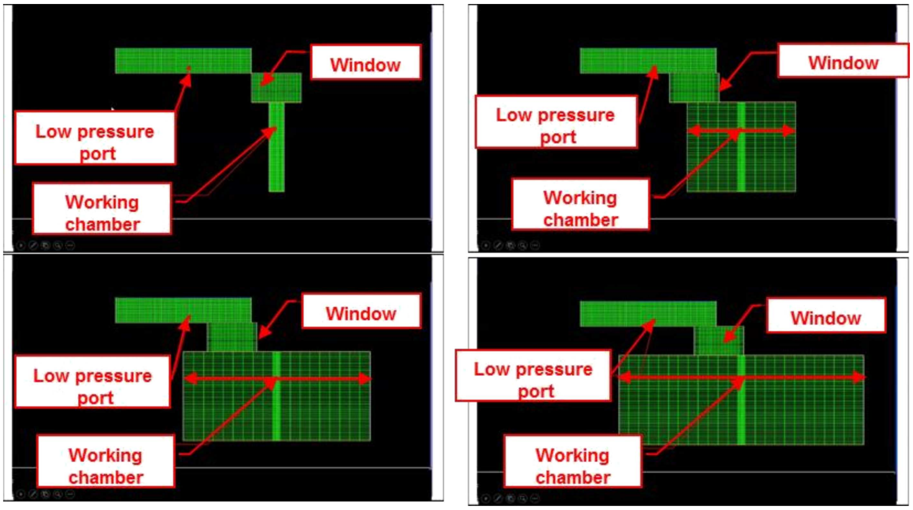

Fig. 7. Meshed axisymmetric model with changing positions of a cam window and pistons.

Oil properties in the CFD model were corresponding to those used in the PWK pump: Azolla ZS 46 with kinematic viscosity at 40°C equal to 46 mm^2/s. Initially the oil density of 880 $\mathrm{kg/m}^3$ was used, with the assumption that the fluid was incompressible. At the end of the pumping cycle the oil in the working chamber, where high pressure is generated by pistons almost touching each other, is discharged to the low pressure port. Because of the fact that the sound wave speed in an incompressible fluid becomes infinitely high such an assumption had to be modified. Otherwise observing sharp pressure changes after the oil is decompressed in the working chamber would not be possible. Therefore a variable oil density dependent on the pressure was assumed and the dependence of oil density on the pressure was derived from the bulk density formula.

Since

$$B = \frac{dp}{\frac{d\rho}{\rho}}, \tag{2}$$

thus

$$d\rho = dp\frac{\rho}{B}, \tag{3}$$

where B – the bulk modulus [MPa], $d\rho$ –the change of fluid density, ρ – the initial fluid density [kg/m^3].

The speed of sound wave could be calculated according to the formula

$$c = \sqrt{\frac{B}{\rho}}. \tag{4}$$

After adjusting the model the predicted sound wave propagation was observed (see Fig. 8).

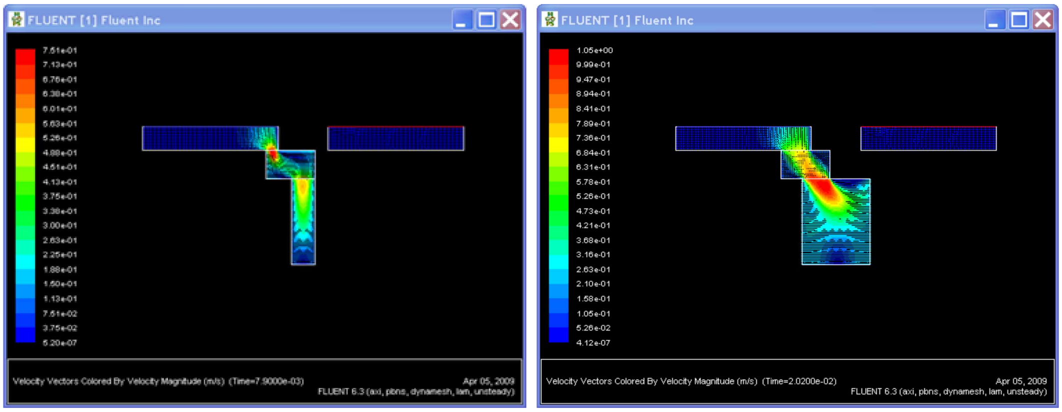

Velocity Vectors Colored By Velocity Magnitude (m/s) (Time=7.9000e-03)
Apr 05, 2009
FLUENT 6.3 (axi, pbns, dynamesh, lam, unsteady)

Velocity Vectors Colored By Velocity Magnitude (m/s) (Time=2.0200e-02)
Apr 05, 2009
FLUENT 6.3 (axi, pbns, dynamesh, lam, unsteady)

Fig. 8. Oil velocity vector distribution at the moment of connecting the working chamber with the low pressure port.

Having proven the appropriate behaviour of the 2D model, the 3D CFD model of the pump was created. There were several configurations of it, but the most used was a 2 chamber model, which comprised working chambers located at the opposite sides of the pump body (Fig. 9). Comparison of results of pressure in selected chambers demonstrated a very close agreement and prompted the use of a smaller model which was easier to handle.

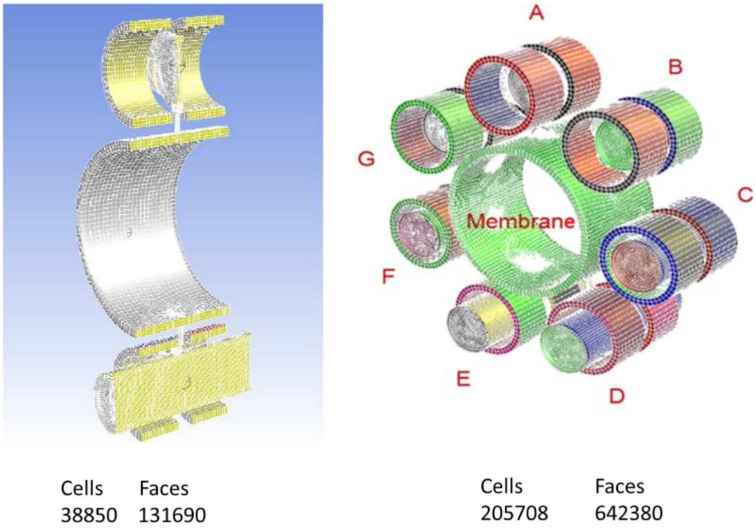

Fig. 9. CFD models considered: 2-chamber symmetric model (left) and 7-chamber full model of the PWK-type pump.

6. Pressure peak elimination by implementing a compensation chamber

As mentioned earlier in instances when the pump displacement varies from 100% there is a possibility of occurrence of pressure peaks in the working chamber which impose risk to pump elements and are accompanied by the increased level of noise. The intensity of those events depends on the pump displacement set by the cam rotational position on the drive shaft, rotational speed of the drive shaft and the oil viscosity. Figure 10 shows the comparison of pressure peaks at different pump displacement settings in the pump working at 100 rpm with high pressure set to 9 MPa. At 100% displacement (top pressure diagram) the pressure distribution follows almost an ideal rectangular shape. By rotating a commutation cam on the shaft to a position corresponding to 20% displacement the pressure response changes and at the end of the pressure cycle there occurs a peak with a magnitude of 5 MPa. An increase in pump rotational speed to 500 rpm with other parameters unchanged (20% displacement and 9 MPa pressure) results in the exacerbation of that effect which is shown in Fig. 11. The amplitude of the pressure peak reaches 26 MPa. An increase of rotational speed to 1000–1500 rpm could cause a significant augmentation of the instantaneous pressure value which could lead to the pump damage.

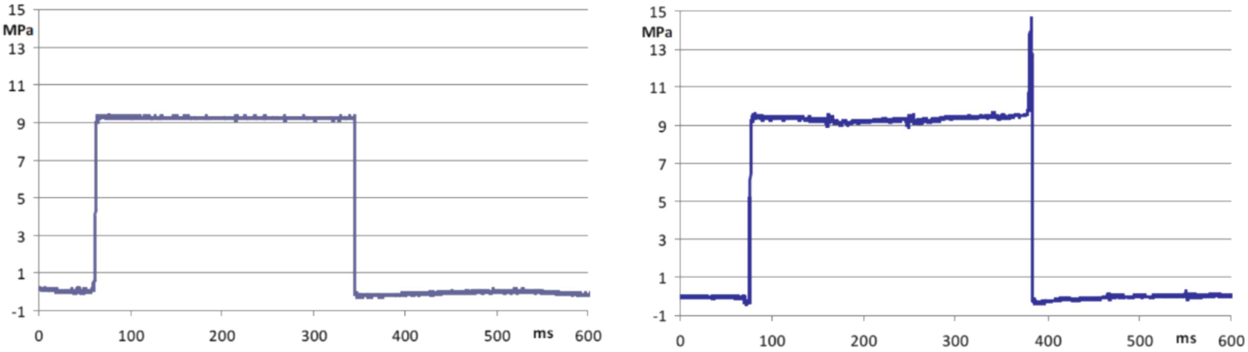

Fig. 10. Pressure changes in a working chamber at different displacements: 100% (left), 20% (right). Pump speed equal to 100 rpm.

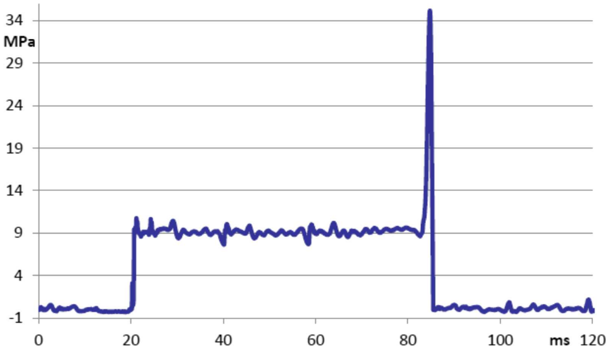

Fig. 11. Pressure distribution in the working chamber of the pump at 500 rmp and 20% displacement.

Therefore a concept of a compensation chamber with an elastic wall was put forward. The chamber is formed by 20 mm-wide groove machined in the pump body. That cavity is constrained by the external wall of a bushing pressed into the body. A bushing has a wall 1 mm thick. There exists a clearance between the drive shaft and the internal wall of the bushing. The compensation chamber is connected with 7 working chambers equally spaced along the perimeter of pump body by means of small orifices. When a working chamber experiences a rapid increase of pressure caused by cutting off the commutation window from either inlet or outlet pressure ports the oil is escaping through the connecting orifices to the compensation chamber that is to absorb an additional oil volume thus decreasing the pressure peak. Since the compensation chamber is simultaneously connected to all working chambers it can equalize pressure in all working chambers.

Figure 12 shows a pictorial rendering of the membrane.

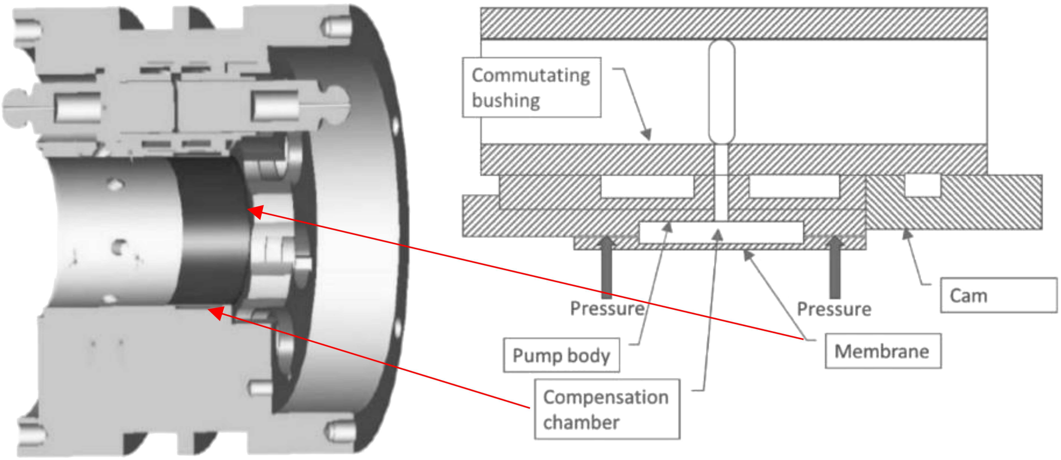

Fig. 12. A design draft of a membrane and the compensation chamber.

A model of the compensation chamber was implemented in the original CAD model of the pump as shown in Fig. 13 and subsequently was subjected to analysis considering the dependence of possible leakage on an interference fit. Contact analysis was conducted on an axisymmetric model.

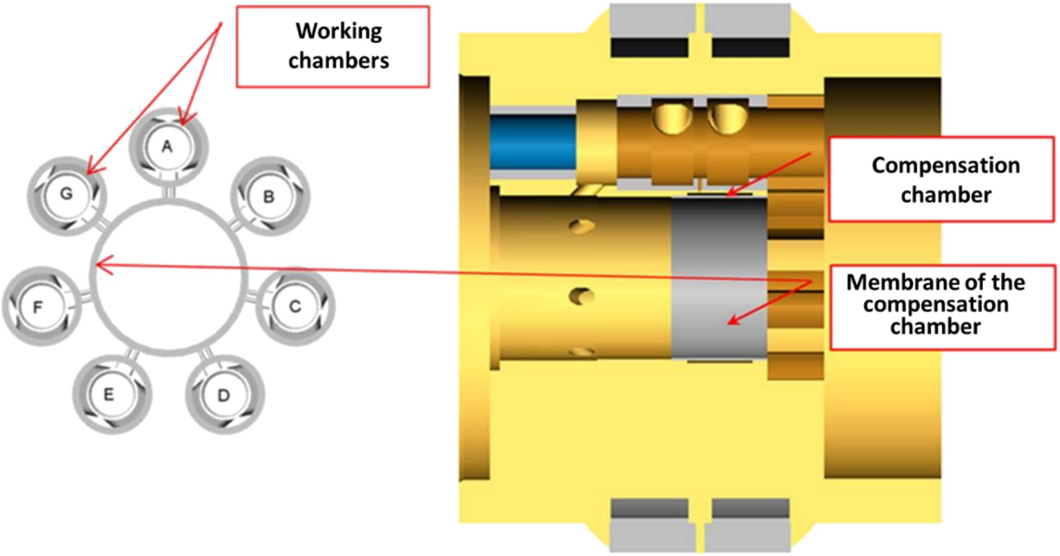

Fig. 13. A cross section of the pump body showing the compensation chamber.

Boundary conditions (loads and support) of the membrane model are shown in Fig. 15. Several values of interference were considered while checking the correlation between the loss of contact and the value of interference at the pressure in the working chamber equal to 45 MPa. Calculations were carried out in several steps, first imposing radial interference and then adding pressure load on the membrane thus creating conditions to check the status of contact between the membrane and the body at the maximum working pressure.

Contact analysis was defined with CONTA172 elements. Those elements are used to model contact and slip between the target surface and other deformable surfaces. The element has 2 degrees

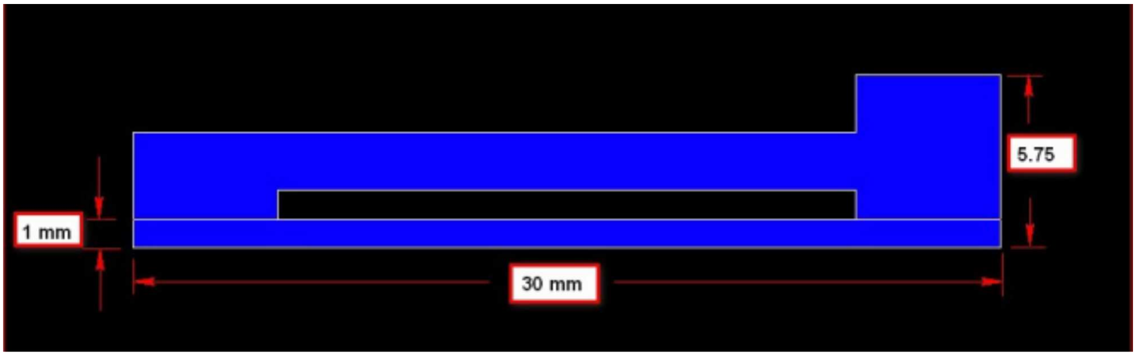

Fig. 14. Dimensions of an axisymmetric model of the membrane.

of freedom in every node: translations in x and y directions. Contact will occur when the element of the target surface is penetrated by the element from the contact pair.

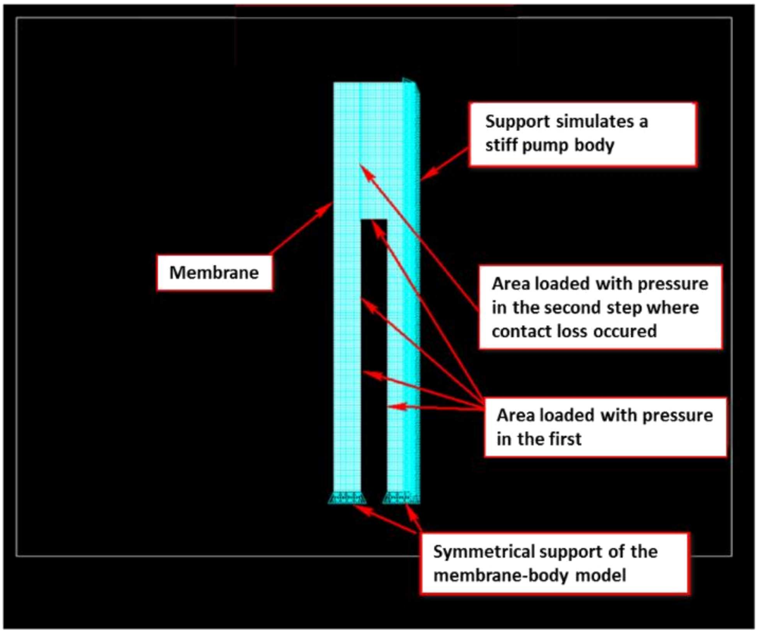

Fig. 15. Axisymmetric model of the membrane-body system.

6.1. Calculation results of the axisymmetric analysis

Figures 16 to 18 show the results of the axisymmetric analysis of a membrane pressed into a pump body with the interference of 0.06 mm.

Received results were verified with the closed form expression (5) by estimating hoop stresses

$$\sigma_h = \frac{PD_M}{2t}, \tag{5}$$

where P – pressure exerted on a wall, t – is the wall thickness, D_M – an average diameter (equal to an external diameter minus t).

Assuming $P = 45$ MPa, $D_m = 52$ mm and $t = 1$ mm we get $\sigma_h = 1170$ MPa. The analysis results showed that a proposed interference of 0.06 mm between the pump body and the bushing with 1 mm thick wall meets the requirement of uninterrupted contact under the maximum pressure load

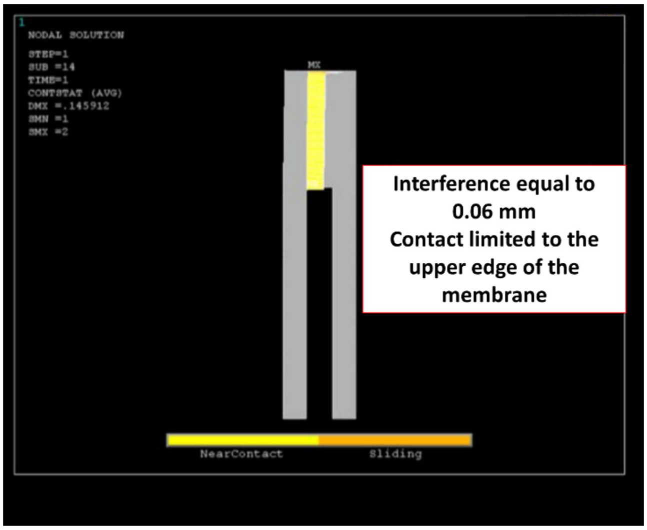

```
1
NODAL SOLUTION
STEP=1
SUB =14
TIME=1
CONTSTAT (AVG)
DMX =.145912
SMN =1
SMX =2
```

Interference equal to
0.06 mm
Contact limited to the
upper edge of the
membrane

Fig. 16. Contact of the membrane with the pump body at the load of 45 MPa acting on the membrane.

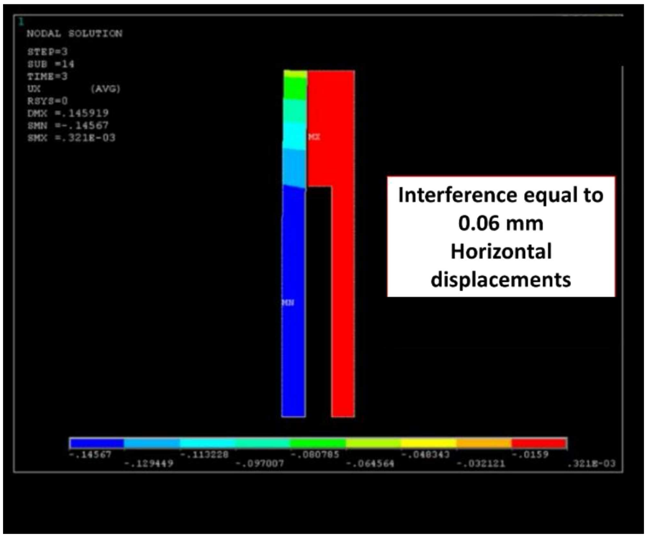

```
1
NODAL SOLUTION
STEP=3
SUB =14
TIME=3
UX          (AVG)
RSYS=0
DMX =.145919
SMN =-.14567
SMX =.321E-03
```

Interference equal to
0.06 mm
Horizontal
displacements

Fig. 17. The displacement of he membrane in the pump body caused by the pressure load.

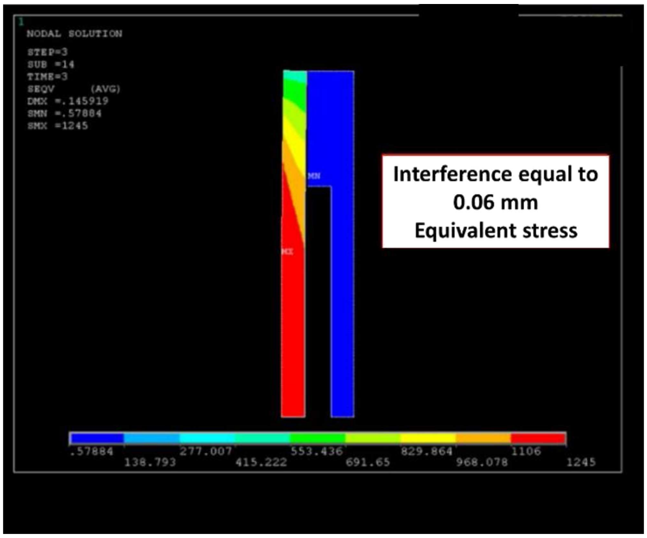

```
1
NODAL SOLUTION
STEP=3
SUB =14
TIME=3
SEQV        (AVG)
DMX =.145919
SMN =.57884
SMX =1245
```

Interference equal to
0.06 mm
Equivalent stress

Fig. 18. Equivalent stress in the membrane subjected to pressure load.

of 45 MPa and stipulates that the membrane has to be manufactured from high strength alloy steel like maraging steel.

Several variants of steel bushings whose walls were selected to serve as compensation chamber membranes were evaluated. A bushing with an inner diameter not much larger than that of the drive shaft whose diameter measured 50 mm was pressed into the cast iron pump body and its external surface was to act as the membrane, forming the bottom part of the compensation chamber. Different configurations of bushings forming compensation chambers are shown in Fig. 19.

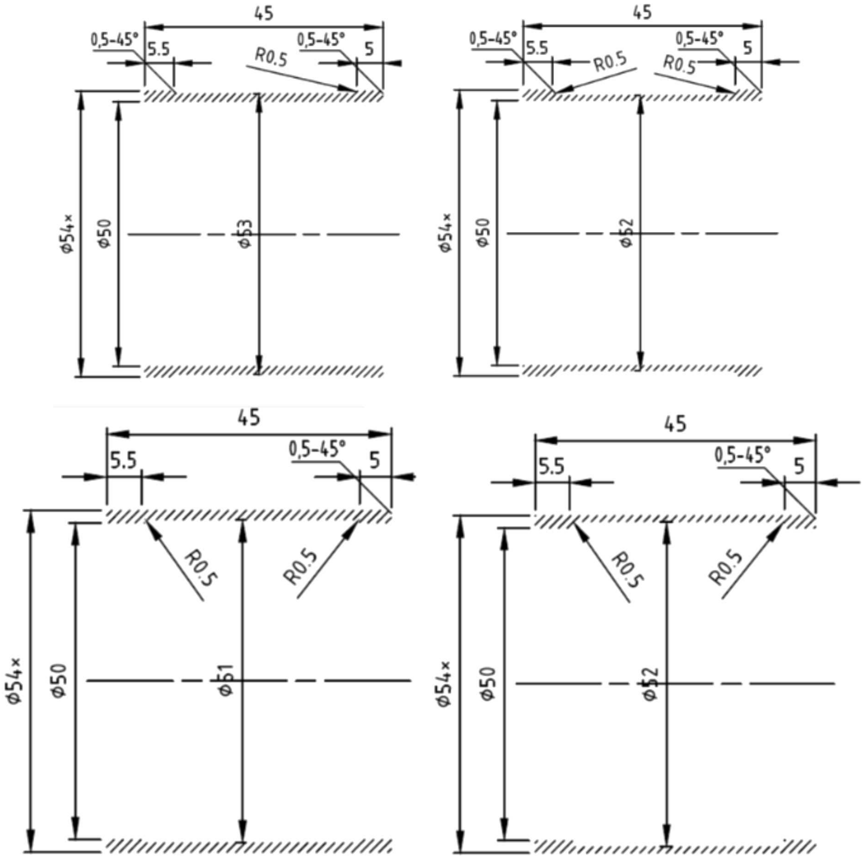

Fig. 19. Different configurations of a compensation membrane.

Allowable displacement of a compensation membrane is limited by a clearance between the membrane wall and the drive shaft. Assuming a thickness of a membrane to be 1.5 mm the radial gap will be equal to 0.4 mm in pump PWKZ-95 and 0.35 mm in pump PWKZ-80.

That clearance seems to be adequate compared to real deformation of the membrane which is at the level of several hundreds of a millimetre. To make that deformation bigger the membrane wall thickness would have to be decreased. Therefore the following options were considered for the membrane wall thickness: 0.6 mm, 0.8 mm and 1 mm. Using formula (5) hoop stress values were calculated for different membrane thickness and pump pressure and are shown in Table 2.

Table 2. Circumferential stresses for bushings of different wall thickness.

P [MPa]	Wall thickness [mm]	Circumferential stress [MPa]	P [MPa]	Wall thickness [mm]	Circumferential stress [MPa]
10	1	247	45	1	113
10	0.8	308	45	0.8	1385
10	0.6	409	45	0.6	1840

The results shown in Table 2 consider a bushing with the internal radius of 24.23 mm. Stresses of that level can be withstood by martensitic steels (see Table 3).

Table 3. Mechanical properties of the heat treated maraging steel. Source: [12].

Grade	Heat treatment	Tensile strength [MPa]	Yield strength [MPa]	Elongation [%]
18Ni (200)	A	1500	1400	10
18Ni (250)	A	1800	1700	8
18Ni (300)	A	2050	2000	7
18Ni (350)	B	2450	2400	6
18Ni (cast)	C	1750	1650	8

A: solution treat 1 h at 820°C, aging 3 h at 480°C; B: solution treat 1 h at 820°C, aging 12 h at 480°C; C: anneal 1 h at 1150°C, aging 1 h at 595°C, solution treat 1 h at 820°C, aging 3 h at 480°C.

An issue of pressure peak compensation in PWK-type pumps was analyzed [9]. After a preliminary research concerning the sensitivity of pressure peaks to pump displacement it turned out that there is no additional value in having a compensation chamber in pumps working at 100% displacement, since no pressure peaks were observed for that setting (see Fig. 10). It holds that the pressure peaks increase with the increase of drive shaft speed for pump displacement settings different than 100%. The comparison of results for different shaft speeds at the same displacement setting and the same pump pressure is therefore valid (see Figs 10 and 11).

The experiments using the following parameters: rpm = 500 and pump displacement = 20% produced pressure plots shown in Fig. 20.

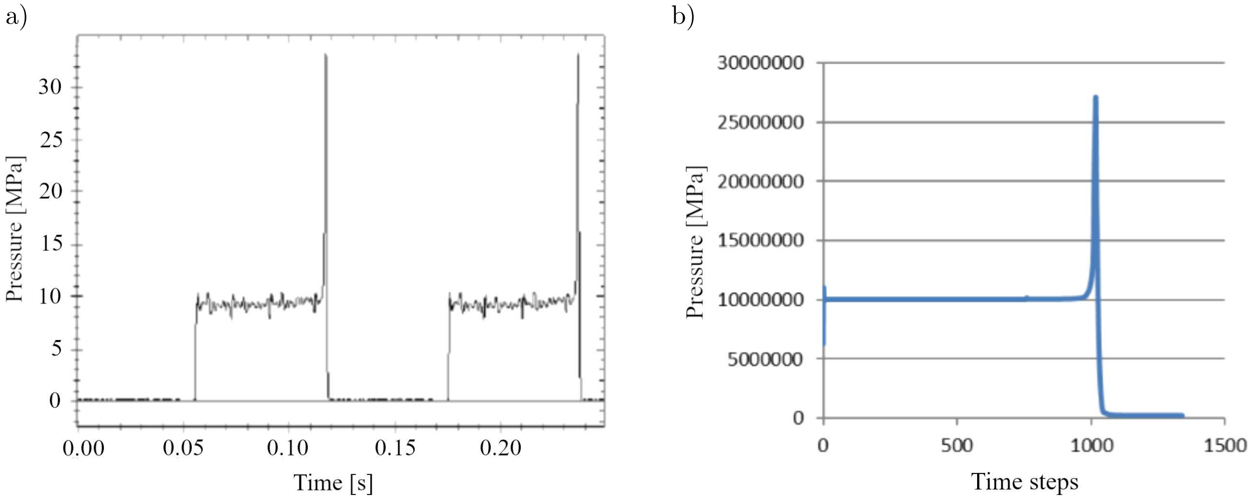

Fig. 20. Pressure peaks in the compensation chamber (20% displacement, 500 rpm): a) experiment results, b) simulation.

The pressure plot shows rapid pressure peaks that correspond to instances when the working chamber access to either pressure port is blocked. If the nominal pumping pressure is set at 10 MPa (as shown in Fig. 20), then the pressure peak will reach a value about 3 times as high. Considering the stress capacity shown in Table 2 and the fact that the pump was designed for pressures up to 45 MPa and drive shaft speeds of 3000 rpm, one has to eliminate thin walled membranes from the design, since they would not meet strength requirements. One advantage of simulation over the experimental tests was the innocuous impact of results on the designed prototype. In performed experimental tests the drive shaft speed was limited out of fear of the pump prototype damage, since increasing the number of revolutions per minute at low displacement settings could result in pressure peaks damaging to pump components. Such a simulation was conducted at 1500 rpm and 20% displacement. The resulted pressure peak would reach values close to 50 MPa at the nominal pump pressure of 10 MPa. The analysis of different cases and requirements for displacement and shaft speeds pointed to the range of 5 MPa as the top peak pressure value, that could be handled by 1 mm thick membrane and the pump offering optimal design parameters. The CFD runs described so far dealt with rigid bodies. In order to get more realistic results Fluid Structure Analysis was conducted so to disclose the response of the membrane that would react to oil pressure. The FSI model was based on one-directional analysis using ANSYS Workbench. The calculations were carried out for the pump pressure of 10 MPa. Figure 21 shows the loading on the compensation chamber membrane and the stress distribution in the membrane.

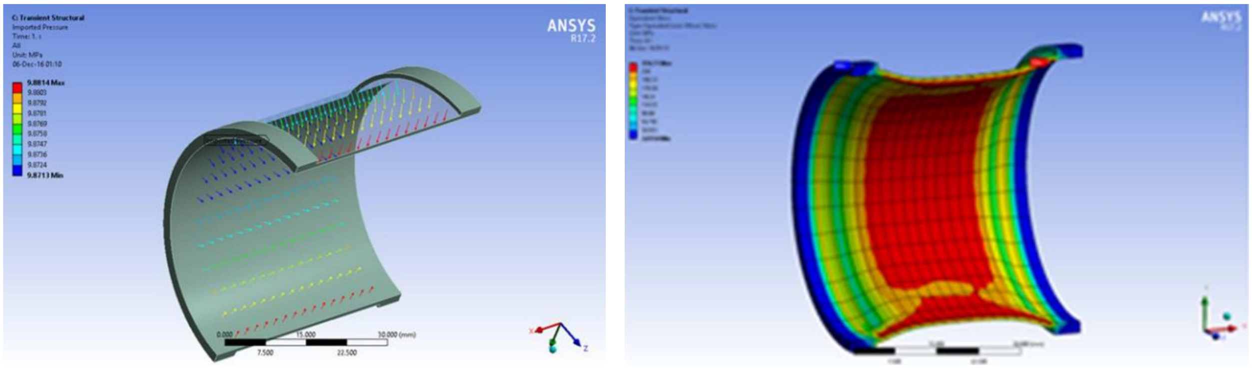

Fig. 21. One-directional analysis of loading by oil pressure on the membrane of the compensation chamber for 1 mm thick membrane and the nominal pump pressure of 10 MPa.

Because of small membrane deformations caused by an interaction of oil with the pump structure the decision was made to drop bi-directional FSI analysis, since its usefulness was questionable.

Summing up analyses and the test results related to the effectiveness of the compensation chamber it looks that the effectiveness of the compensation chamber, in certain displacement ranges, was due to the compressibility of oil rather than the deformation of the membrane. It seems that the membrane of the compensation chamber is not capable of eliminating satisfactorily pressure peaks in the working chamber of variable displacement pumps working at high speeds. That means that the alternative approach is needed to achieve that goal.

7. Pressure peak elimination by cam profile optimization

To address still another option of eliminating pressure peaks in the working chamber, namely reducing the working chamber cut-off time, the designers looked into increasing the speed of the commutation bushing by optimizing the shape of the cam profile. The procedure of cam profile selection and calculations connected with it was described in [6]. One of the most important parts of the commutation mechanism shown in Fig. 3 is a commutating bushing driven in a reciprocating motion by the axial cam mounted on a drive shaft and rotating with it. In the middle of each bushing length there are 3 circumferential cuts of width b_o which act as commutation windows. They alternately connect a working chamber (which is defined by the faces of both opposite pistons and the inner surface of the bushing) with low and high pressure ports. Those ports are separated by a “bridge” of the width b_m. As in the case of the valve commutation plates, the width of the bridge has to be greater than the width of commutation windows in a bushing, which results in a temporary cut off between a working chamber and pressure ports (both high and low).

The basic factor which controls the character of bushing motion is the curvature of the commutation cam profile. That profile assures the full reciprocating motion with a period equal to a full rotation of the drive shaft and small amplitude. The simplest example of a cam meeting such requirements is a cam with a sinusoidal profile. The equation of motion of a bushing driven by a cam is as follows

$$x_r = s_r \sin \varphi_w, \tag{6}$$

where s_r is the amplitude of the cam profile curvature, while φ_w is the angular position of the drive shaft. The motion of pistons moving in the commutation bushing differs from the motion of the bushing in amplitude as well as phase, which is equal to $\pi/2$.

That is an essential condition for the pump with cam commutation to achieve maximum displacement.

The general equation describes the motion of the commutation bushing:

$$x_r = s_r Z(\varphi_w), \tag{7}$$

where $Z(\varphi_w)$ is the shape function of the cam. The cam has to comply with several criteria one of them being the minimal time to switch from the position when the working chamber is connected with one pressure port to the position corresponding with the connection to an opposite port. During that time a temporary cut off of the working chamber from pressure ports takes place which causes undesirable pressure peaks in the chamber. They are the source of noise and vibration and could affect pump efficiency and its durability. Time of the cut off could be defined by an angle by which the drive shaft will turn.

The duration of the working chamber cut off is defined by the rotation angle of the drive shaft corresponding to the linear translation of the commutation bushing by a distance equal to $\Delta b_m = b_m - b_o$. Figure 22 shows: a) the process of an instantaneous cut off of the working chamber when the window is covered by the "bridge" between pressure ports and b) the dependence of the cut off angle on the cam curvature profile. At the same time the cam profile should minimize acceleration and mass forces acting on the components of the commutation mechanism during all stages of their motion. That means that values of the second derivative of the cam profile shape function $\ddot{Z}(\varphi_w)$ should be minimized. The last assumed criterion of the profile curvature usefulness is the minimal value of the cam profile curvature radius at an arbitrary point of the profile. Considering all above criteria a cam profile curvature defined by the power function was

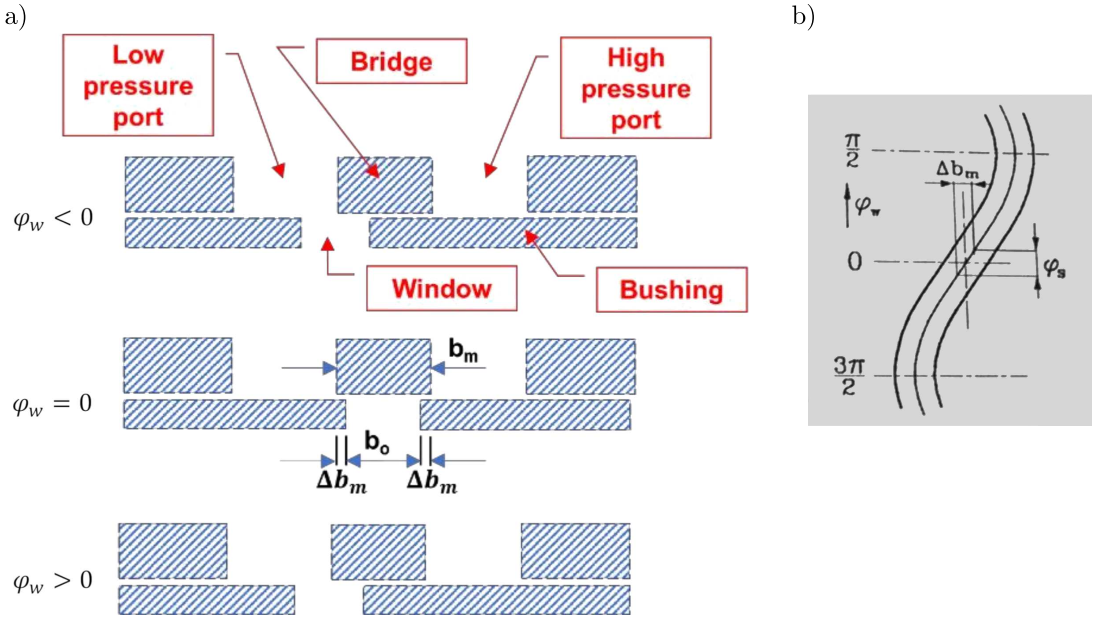

Fig. 22. Temporary cut off of the working chamber from pressure ports.

proposed. In the pump PWK 80 the profile was described by the following equations which defined profile curvature in the specified angular intervals of the drive shaft revolution

$$0 \le \varphi_w \le \frac{\pi}{2}, \qquad y = 4.5\left[1 - 0.32337\left(\left(\frac{\pi}{2} - \varphi_w\right)^{2.5}\right)\right] + 0.5\sin\varphi_w, \tag{8}$$

$$\frac{\pi}{2} \le \varphi_w \le \pi, \qquad y = 4.5\left[1 - 0.32337\left(\left(\varphi_w - \frac{\pi}{2}\right)^{2.5}\right)\right] + 0.5\sin\varphi_w, \tag{9}$$

$$\pi \le \varphi_w \le 3\frac{\pi}{2}, \qquad y = 4.5\left[0.32337\left(\left(3\frac{\pi}{2} - \varphi_w\right)^{2.5}\right) - 1\right] + 0.5\sin\varphi_w, \tag{10}$$

$$3\frac{\pi}{2} \le \varphi_w \le 2\pi, \qquad y = 4.5\left[0.32337\left(\left(\varphi_w - 3\frac{\pi}{2}\right)^{2.5}\right) - 1\right] + 0.5\sin\varphi_w. \tag{11}$$

In order to evaluate the velocity of the bushing a CFD model of the pump with the cam having a curvature profile described by Eqs (8)–(11) was created. Since the values of analytically defined power functions at the end of intervals were discontinuous – numerical solution was used to define a smooth profile function. An algorithm was written in the C language and it considered function singularities. It was also used to define the speed of the commutation bushing by differentiating the profile shape function for every interval separately. The algorithm was compiled and used as a User Defined Function in the run of the CFD model using ANSYS Fluent. Profiles of cams described by power and sinusoidal functions are shown in Fig. 23.

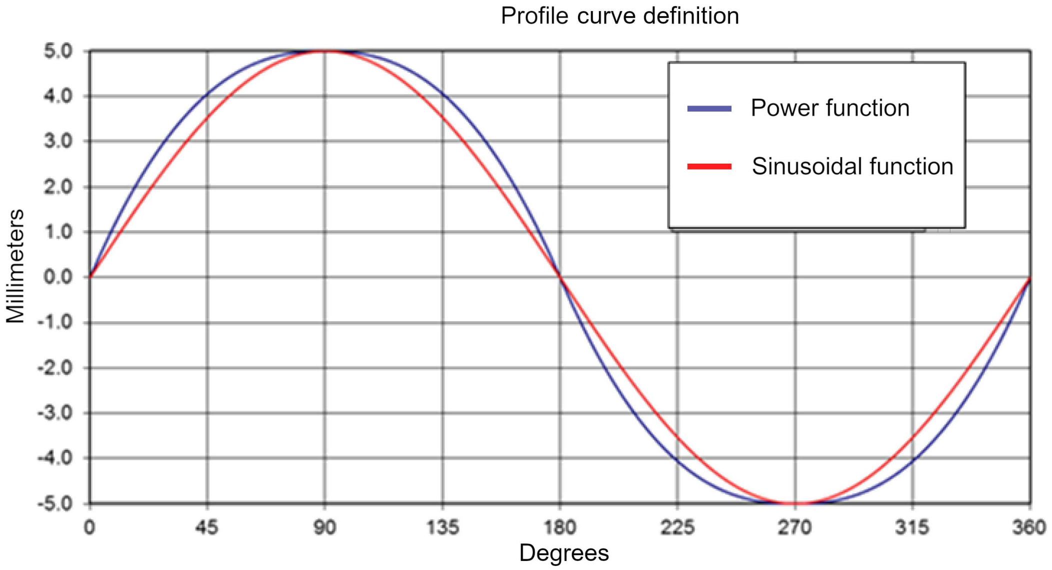

Fig. 23. Comparison of cam profile curvatures described by different functions.

The commutating bushing speed was recorded during a model analysis and subsequently compared with results of the run based on a model defined by a sinusoidal cam. The comparison of those results is shown in Fig. 24. Comparing the cam profiles and speed plots brings the following remarks: attempts were made to arrive at an optimized cam profile that would assure the increase of the bushing speed in order to attain the shortest cut off time of the working chamber and would not excessively increase the acceleration and constrain the curvature of the cam profile. Figure 24 shows sharp changes of bushing velocity driven by the cam defined with a power function. They are caused by function discontinuity at every quarter of the pump cycle. According to the pump designer rounding off the profile shape function in the discontinuity points can adversely affect the value of acceleration – which will cause the increase of forces acting on the bushing and can also affect the curvature of the profile which should not be too small.

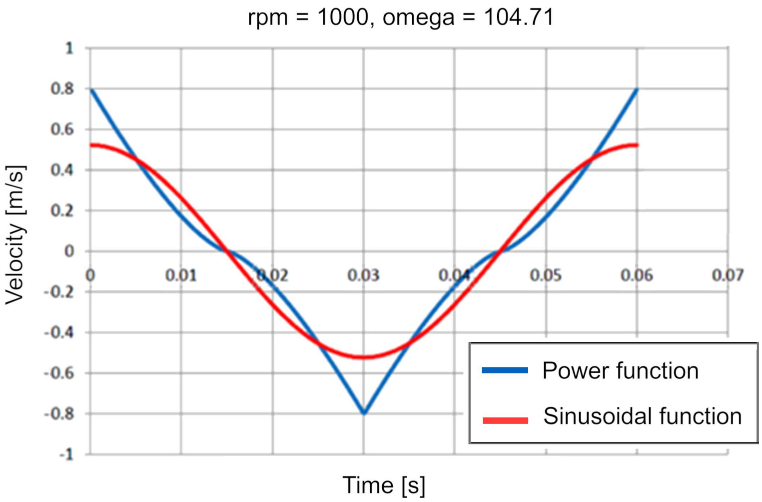

Fig. 24. Comparison of bushing velocities for cam profiles described by different functions.

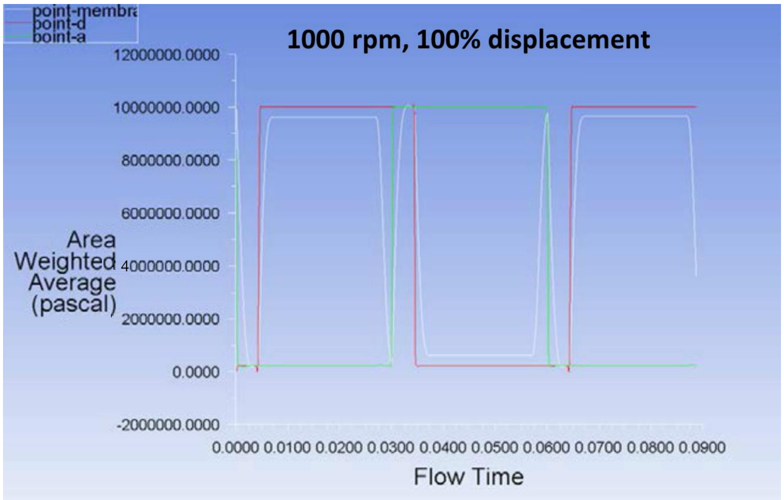

Fig. 25. Pressure in the pump driven by the cam defined with a sinusoidal function.

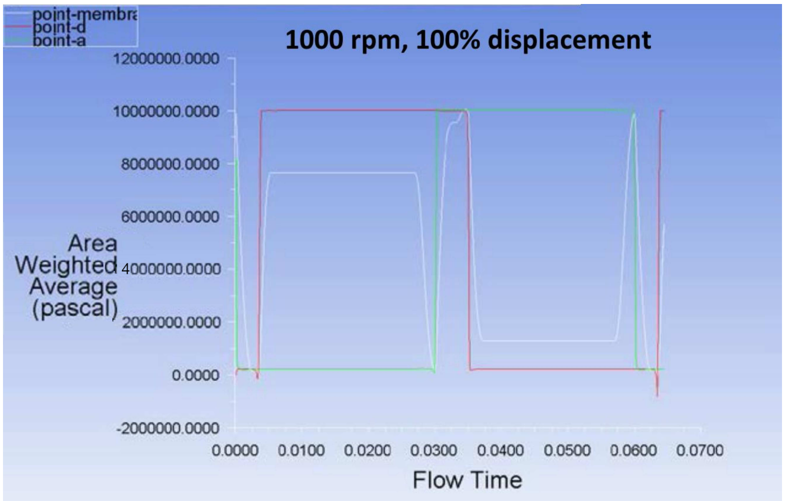

Fig. 26. Pressure in the pump driven by the cam defined with a power function.

The analysis of fluid models with respect to pressure in the pump chambers showed that the pressure in the compensation chamber does not “keep up” with the pressure in the working chamber when the commutation mechanism is driven by a cam whose profile is defined with the power function (Figs 25 and 26). The conclusion of the analysis prompted the decision to concentrate on cams defined by a sinusoidal function.

8. Pressure peak elimination by reconfiguring the compensation orifices

Because described attempts to eliminate pressure peaks did not turn out to be efficient still another solution was considered: to increase the area of compensation orifices connecting working chambers placed circumferentially with the centrally located compensation chamber. Initial experiments were started with single orifices of small diameters, subsequently changing both the number of orifices and their size. The disadvantage of such experimental approach having only one pump prototype was clear: there was no “way back” to previous orifice configurations if a need aroused to compare results with a later-made change. Here simulations were handy to make different comparisons of any configurations. And some simulation results indicated that with small enough orifice area throttling of fluid may occur which could cause cavitation. Therefore simulation runs were carried out in order to assess the possibility of cavitation occurrence.

8.1. Cavitation model

Cavitation is a process of discontinuation of fluid flow due to the decrease of pressure and the formation of bubbles filled with gas. Cavitation can occur in two forms: vapour and gas. Vapour cavitation is a boiling process in which a rapid volume growth occurs during the transformation of liquid into vapour. Such a situation will take place when the pressure falls below vapour pressure of the liquid. Gas cavitation is a diffusive process which will occur when pressure falls below the saturation pressure of gases solved in the liquid. While the vapour cavitation is very violent and it can last microseconds, gas cavitation is much slower. Damage is usually caused by vapour cavitation when the shock wave can cause erosion of a surface. Gas cavitation is responsible for noise generation, rise of temperature and oil degradation through oxidation. In hydraulic pumps, where the hydraulic oil is an energy transporting medium there occurs cavitation connected with the release of dissolved gas from oil. Gas bubbles created by a local drop of pressure are transferred by oil to the area of higher pressure, where they implode. The pressure level in a suction duct of the pump ((5–10)10^3 Pa) is much higher than the vapour pressure of mineral oil ((0.1–1)10^3 Pa) in the operational temperature range of the pump. Solvability of air in the oil could be from 6 to 12%, while the solvability of air in the water at 293 K equals to 1.6%. Bigger solvability of air in the hydraulic oil and smaller vapour pressure makes cavitation bubbles formed in the hydraulic oil filled almost entirely with air. Traces of oil vapour occur only in oils of small viscosity at the temperature above 350 K and elevated values of under pressure, when most volatile fractions of oil evaporate. In water cavitation occurs more easily and bubbles are filled with water vapour. Harmfulness of cavitation can be manifested by:

- incomplete filling of working chambers with hydraulic oil – which lowers the efficiency of the pump;
- occurrence of dynamic phenomena (vibrations) through lowering the elasticity modulus;
- long and persistent cavitation can cause cavitation erosion on metal surfaces;
- noise.

Viscosity of hydraulic oil μ and its dependence on temperature is the basic parameter taken into account when selecting oil for the hydraulic system. Too low viscosity can deprive the fluid its lubrication properties while too high viscosity can cause cavitation. Solvability of air in the hydraulic oil depends directly on pressure in the hydraulic system. In locations where pressure falls rapidly there is a violent creation of air bubbles. Foam that is formed in the areas of a high flow velocity can cause cavitation damage to the surface of pump elements. That phenomenon can be limited by the oil tendency to release air. Some effects caused by air dissolved in oil are shown in Fig. 27.

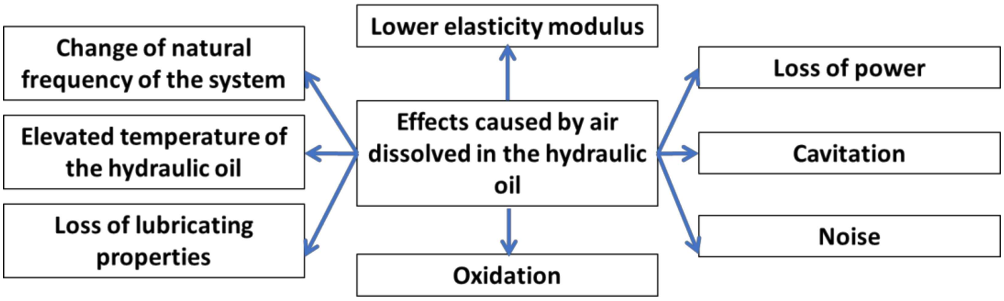

Fig. 27. Harmfulness of air contents in the hydraulic oil.

Surface damage owing to cavitation occurs at the border between the liquid and the structure and is caused by the fact that part of the fluid is subject to the elongation stress which causes boiling of the liquid and subsequently it is exposed to the compression stress which causes violent implosion of gas bubbles. Such implosion causes a mechanical shock (shock wave) and the creation of a cumulative vapour, which impacts the surface at several hundred meters per second. Each flow system exposed to a recurring compressive-tensioning stress is subjected to cavitation damage, which is similar to surface fatigue damage. Materials which are resistant to damage (are hard and tough) are also resistant to cavitation. The dynamics of spherical bubbles filled with air can be described with the Rahyleigh-Plesset equation which is a special case of the Navier-Stokes equation defining the oscillation motion of a spherical bubble suspended in an inelastic fluid. In the linear range the bubbles oscillate harmonically according to so-called the Minnaert resonance frequency. When the oscillations have bigger amplitudes that motion becomes non-linear. As in the case of the Navier-Stokes equation there is no general solution of the Rayleigh-Plesset equation. Spherical bubbles are described by a relation between the radius R of the bubble and the conditions in the gas and liquid. Its simplified version is shown by Eq. (12)

$$\frac{\Delta P}{\rho} = R\frac{d^2R}{dt^2} + \frac{3}{2}\left(\frac{d^2R}{dt^2}\right)^2, \tag{12}$$

where ΔP – a difference between local and global pressure, ρ – the density of the liquid, $\frac{dR}{dt}$ – the rate of growth of bubbles.

A numerical solution of R-P equation has additional terms which define kinematic viscosity of liquid and surface tension. The growth of bubbles takes place in an explosive process in which their volume grows as defined in (13)

$$dR = t^3 dt. \tag{13}$$

For comparison, the growth of a gas bubble radius during the boiling process is equal and is described by (14)

$$dR = \frac{1}{\sqrt{t}}dt. \tag{14}$$

The intensity of cavitation could be described as the product of the gas bubble implosion pressure and the number of bubbles. When the cavitation bubble implodes a pressure pulse is generated which generates noise intensified by the number of bubbles and the magnitude of pressure generated by separate bubbles. It was shown that the acoustic pressure p_0 at the distance ξ from the center of volume V is the function of the second derivative of the volume differential

$$p_0 = \frac{\rho}{4\pi\xi}\frac{d^2V}{dt^2}. \tag{15}$$

Noise generated during the implosion of a gas bubble is defined by the significant term $\dfrac{d^2V}{dt^2}$. The magnitude of implosion pressure P_i mentioned in the scientific literature, rangers from 140 to 690 MPa. Rayleigh calculated the implosion pressure with (16)

$$P_i = \sqrt{\frac{2}{3}P_o\rho\left(\frac{R_i^3}{R_f^3} - 1\right)}, \tag{16}$$

where c – the speed of sound in the liquid, P_o – undisturbed pressure (pressure of the system), R_i – initial bubble radius, R_f – final bubble radius.

Turbulence was described with the Sparalart-Almaras model. Cavitation can be simulated in several ways.

One of them defines fluid as a mixture of two phases: liquid (formed by the hydraulic oil) and gas. The mixture definition was defined by the Singhal model, also called the full cavitation model. The model considers the change of phase, the dynamics of gas bubbles, turbulent changes of pressure and non-condensable gases. The model solves the continuity equation and momentum equation for the mixture and the volume fraction for the gas phase. It is assumed that oil is a mixture of liquid, vapour and non-condensable gases. The density of mixture depends on mass fraction of vapour γ_v and non-condensable gases γ_g and is calculated from the transport equation coupled with equations of continuity and momentum. The mixture density can be described by (17)

$$\frac{1}{\rho} = \frac{\gamma_v}{\rho_v} + \frac{\gamma_g}{\rho_g} + \frac{1 - \gamma_v - \gamma_g}{\rho_l} \tag{17}$$

and

$$\gamma_v = \frac{a_v\rho_v}{\rho}, \qquad \gamma_g = \frac{a_g\rho_g}{\rho}, \qquad \gamma_l = \frac{a_l\rho_l}{\rho} = 1 - \gamma_v - \gamma_g, \tag{18}$$

where a_g, a_l, a_v denote respectively volume fractions of noncondensable gas liquid and steam, $a = a_g + a_v$ is a total volume fraction of steam.

A mass fraction of vapour is defined by the transport equation

$$\frac{\partial(\rho\gamma)}{\partial t} + \Delta\cdot(\rho\gamma\vec{v}) = \Delta\cdot(\Gamma\Delta\gamma) + R_e - R_c, \tag{19}$$

where $\vec{v}$ the velocity vector of the steam phase, Γ the diffusion coefficient, R_e and R_C coefficients of generation and condesation of steam.

In a liquid in which an interphase slip has been neglected the dynamics of condensation bubbles is described by an equation based on the general Rayleigh-Plesset equation

$$R_B\frac{D^2R_B}{Dt^2} + \frac{3}{2}\left(\frac{DR_B}{Dt}\right)^2 = \frac{P_B - P}{\rho_l} - \frac{4v_l}{R_B}\dot{R}_B - \frac{2\sigma}{\rho_l R_B}, \tag{20}$$

where R_B –bubble radius, σ – liquid surface tension coefficient, ρ_l – liquid density, P_B – bubble surface pressure, P – local far field pressure.

Neglecting the second-order terms and the surface tension force, Eq. (20) is simplified to:

$$\frac{DR_B}{Dt} = \sqrt{\left(\frac{2}{3}\right)\frac{P_B - P}{\rho_l}}. \tag{21}$$

Three cavitation models were considered in the analysis: apart from the Singhal model also Scherr-Sauer and Zwart-Gerber-Belamri models were used [1]. Only the Singhal model was including non-condensable gases (like air) in the mixture. In order to simulate cavitation using two remaining models the following procedure had to be followed: a) 2 species had to be formed within one phase (oil vapour and non-condensable gas or b) an additional 3rd phase had to be created (air) apart from oil vapour and liquid oil. When 3 phases are modelled each of those phases can be presented separately when showing the results of the simulation. That approach was used in order to locate air bubbles in the compensation orifice during discharge of pressure from the working chamber to the compensation chamber. A possibility of cavitation in the PWK-type pump was checked in the modified prototype for the configurationof the compensation orifice of 1 mm diameter because of the biggest flow resistance (Fig. 28).

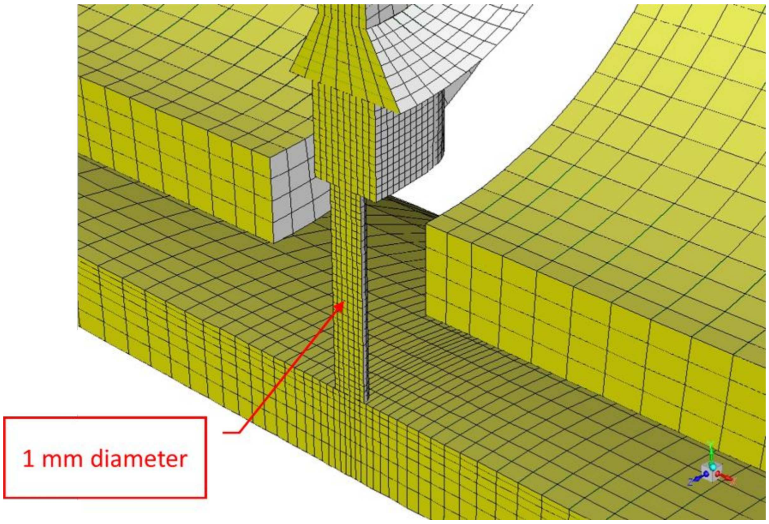

Fig. 28. Symmetric model of the pump with 1 mm diameter compensation orifice.

Figure 28 shows part of the 2 chamber symmetric model of the PWK-type pump. Because of the model symmetry, the compensation orifice is shown in the form of a half cylinder of 1 mm diameter. The pump was working at 1500 rpm, the displacement was set at 100%, the intake pressure level was equal to 0.2 MPa, while the output pressure was defined at 10 MPa. The Azzola ZS 46 oil had the density reference value set at 872 kg/m^3, oil dynamic viscosity $\mu = 0.044$ kg/(m·s), vapor pressure was 1 Pa, dynamic viscosity of oil vapour was 0.00055 kg/(m·s), density of air was assumed as for the ideal gas, oil temperature was 40°C, volume fraction of air in oil was 8%, which corresponds to the mass fraction of air equal to 40 ppm. Cavitation was checked at the instance when the lower commutation bushing was located under the "bridge" separating low and high pressure orifices and was just about to connect with the high pressure port. At that moment lower pistons are still in the suction phase and are moving away from each other creating low pressure in the lower working chamber. When the commutating bushing window moves to the right it connects with the high pressure port and the pressure in the working chamber rapidly increases to 10 MPa. That causes oil to escape to the compensation chamber through the compensation orifice. In order to observe cavitation in the pump, the time step was set at $5 \cdot 10^{-5}$ s and the mesh was adapted by decreasing the cell size in the vicinity of the area where cavitation could be expected.

During discharge of pressure from the lower working chamber to the compensation chamber the hydraulic oil flowing into the compensation orifice can reach the velocity of 140 m/s (Fig. 30).

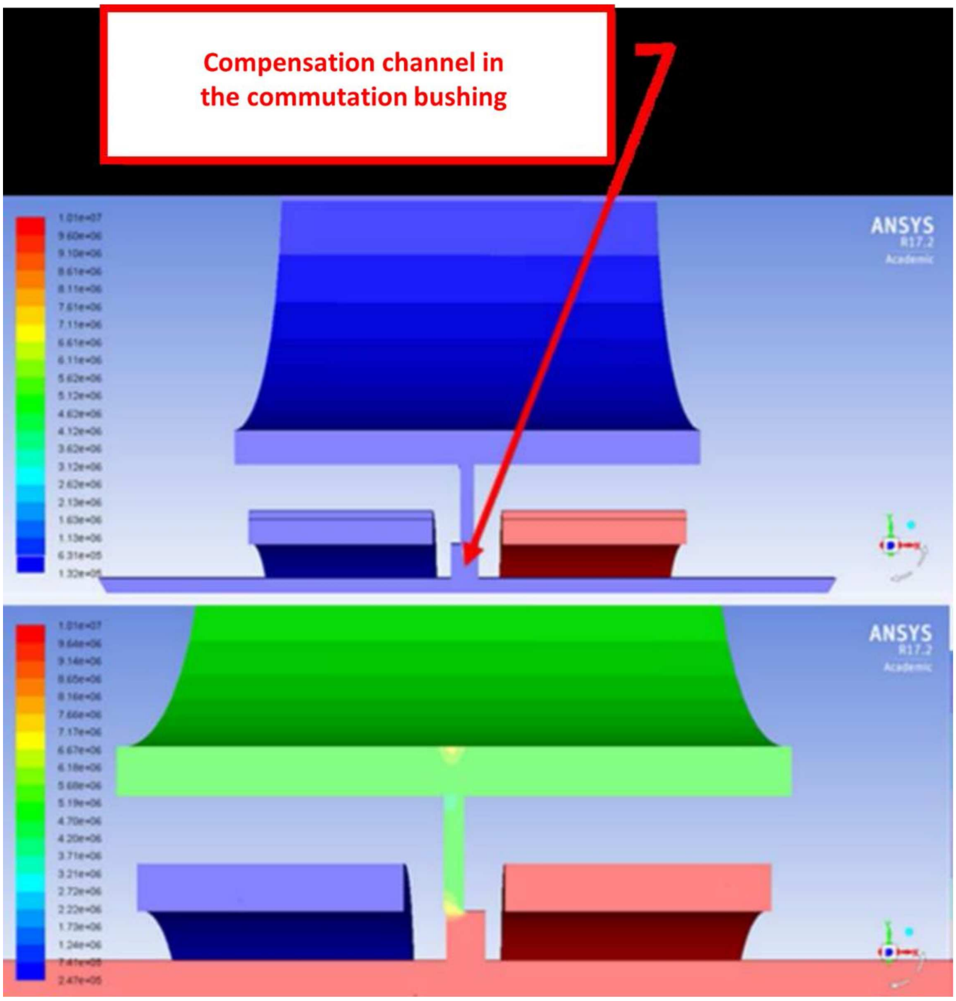

Fig. 29. Change of pressure in the lower working chamber before (top) and after (bottom) lower working chamber is connected to the output port.

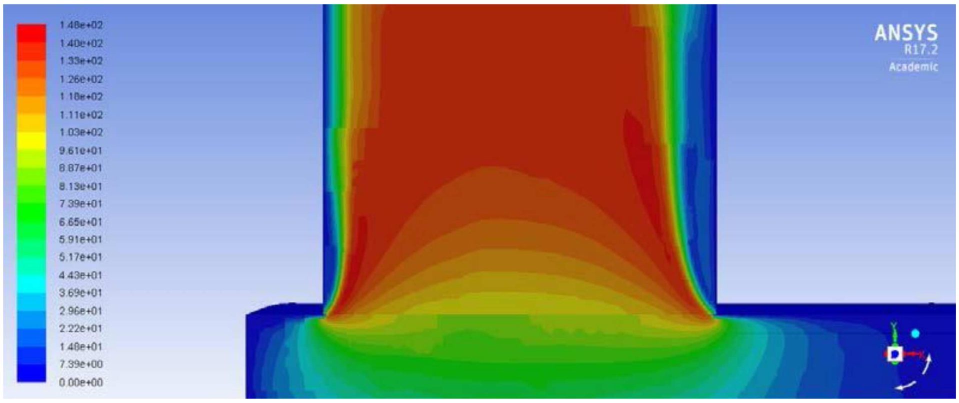

Fig. 30. Velocity contours of oil flowing into a compensation orifice.

A velocity distribution along the whole length of the compensation orifice is shown in Fig. 31.

The Reynolds number reached the value of 443 and its distribution in the lower compensation orifice is shown in Fig. 32.

The absolute pressure check was used to assess the occurrence of cavitation in the compensation orifice. The results are shown in Figs 33 and 34.

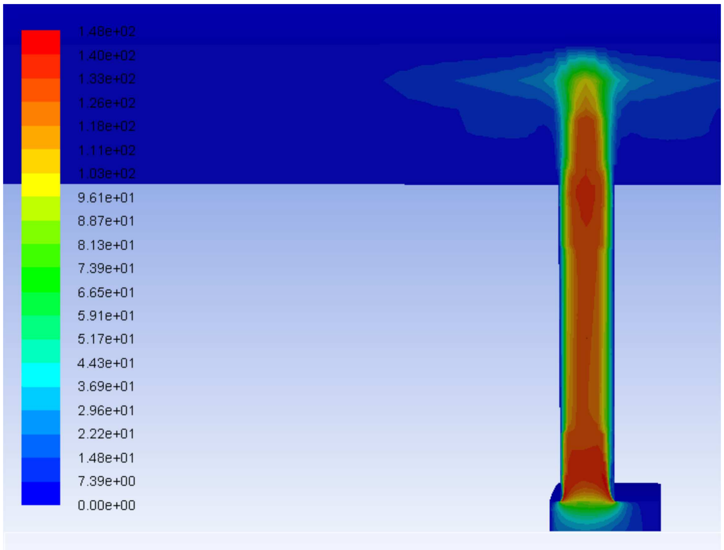

Fig. 31. Velocity contours in the lower compensation orifice during the pressure discharge.

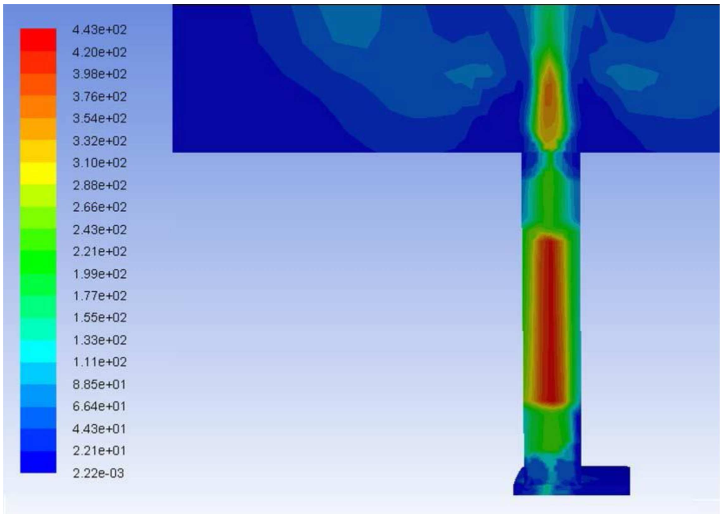

Fig. 32. Reynolds number contours along the cross section of the lower compensation orifice.

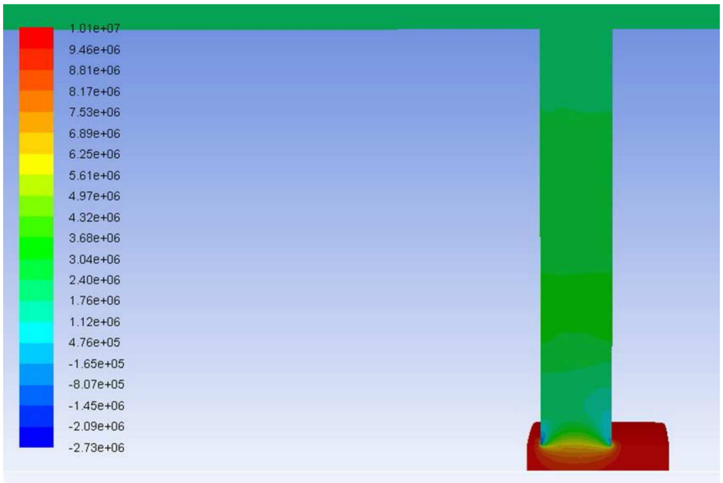

Fig. 33. Contours of absolute pressure [Pa] in the lower compensation orifice.

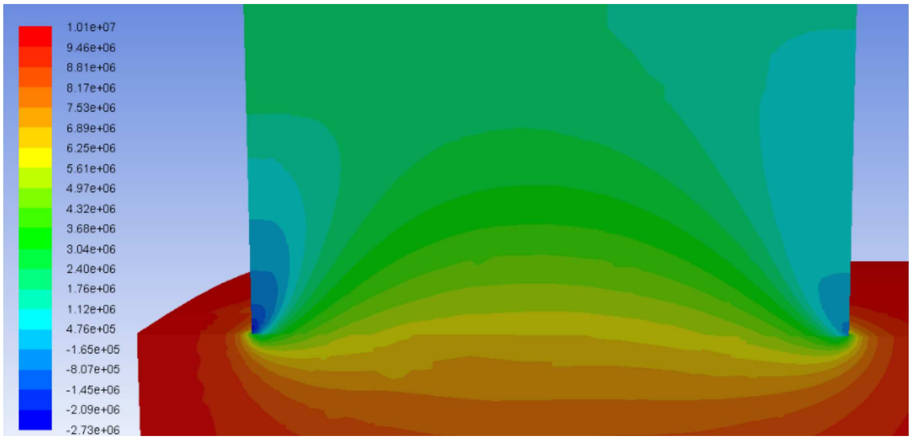

Fig. 34. Contours of absolute pressure at the inlet to the lower compensation orifice.

The cavitation model of Zwart-Gerber-Belamri was used to scrutinize phenomena at the inlet of the compensation orifice. A method defining 3 phases of oil was used: liquid, vapour mixture and non-condensable gas, namely air. That approach allowed to selectively present each phase on a plot. The density of air was defined as the density of ideal gas. It was assumed that the amount of air dissolved in oil is equal to 8% and the vapour pressure of the hydraulic oil is 1 Pa.

The energy equation was turned off, while the continuity, turbulence and transport equations were turned on. The results of calculations of the cavitation model are shown in Figs 35 and 36.

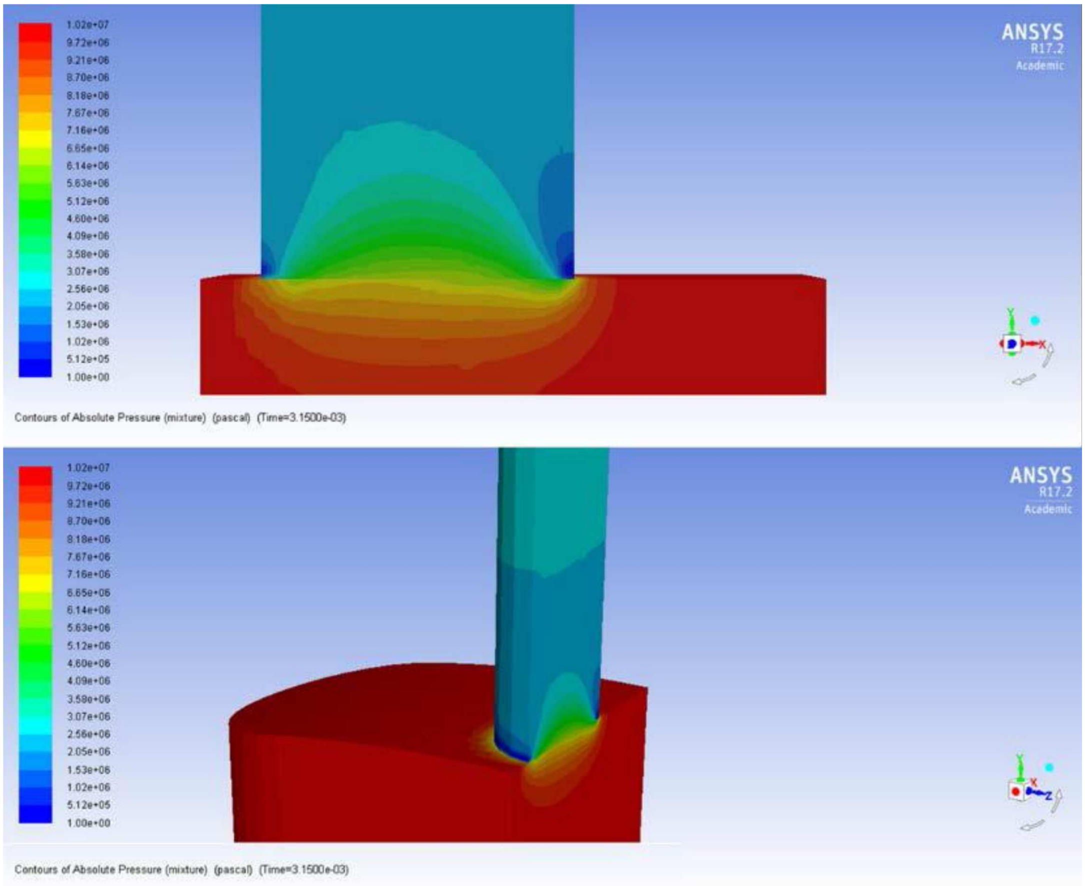

Fig. 35. Absolute pressure contours in the lower compensation orifice shown in a ZGB model (3 phases).

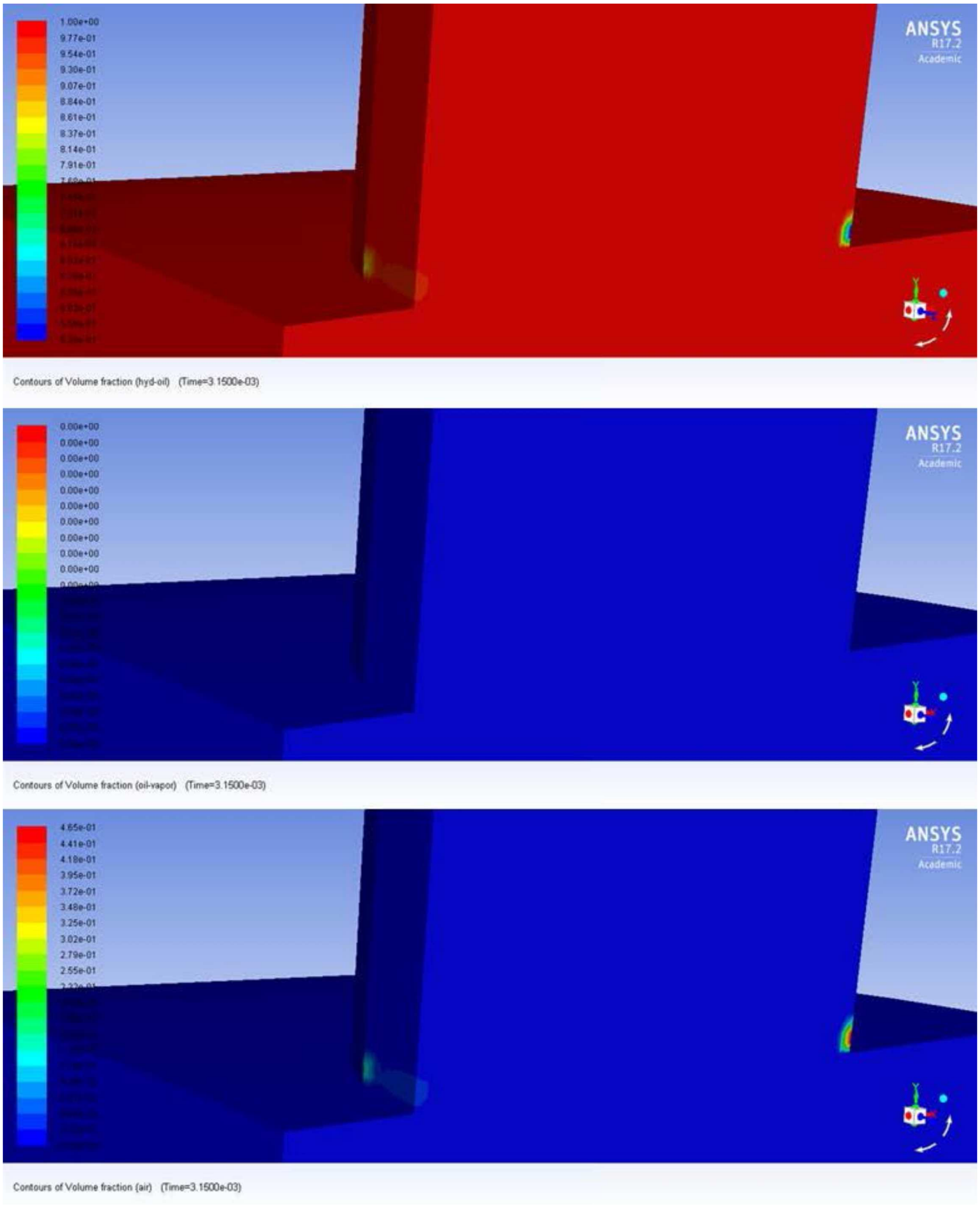

Fig. 36. Contours of volume fraction in the lower compensation orifice in a ZGB model (3 phases).

Figure 35 shows a visible zone of lowered pressure at the area of contact between the inlet of the lower compensation orifice and the outlet of the lower commutation bushing. The value of pressure reaches 766 Pa, which is above the value of vapour pressure for the hydraulic oil (1 Pa) and causes the release of air bubbles from oil. It is shown in Fig. 36 where comparison of volume fractions of all 3 phases is presented. The bottom-most picture in Fig. 36 shows air bubbles in the liquid.

To verify the results shown above an analysis of a cavitation model was carried out with 2 phases defined. The phases were oil and the vapour mixture defined in the ZGB model. In the mixture 2 species were present: hydraulic oil vapour and air. The mixture density was assumed to correspond to that of an ideal gas. The results for both models are very similar. The difference between 2 and 3-phase ZGB models lies in the fact that in a 3-phase model each phase can be selectively chosen

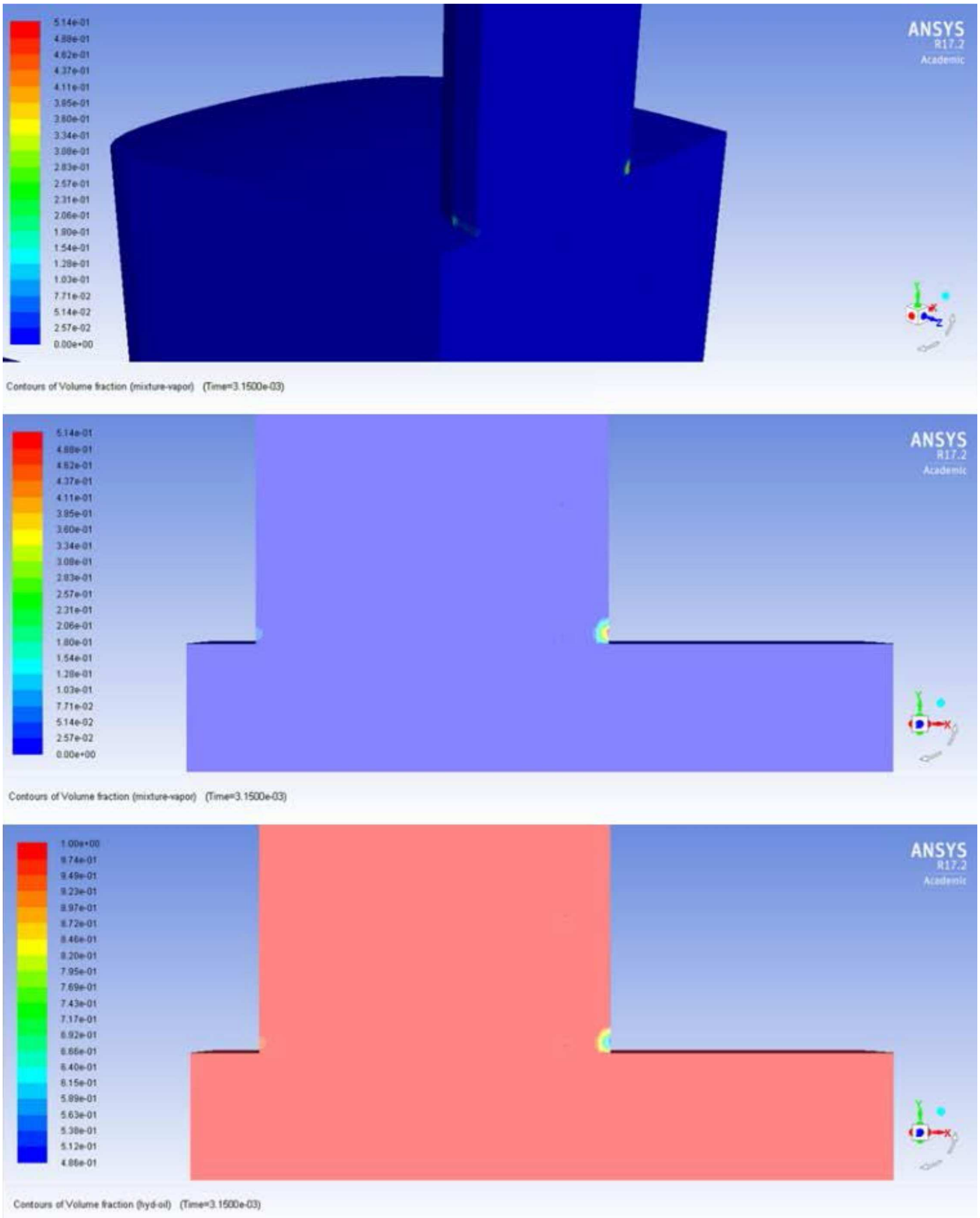

Fig. 37. Volume fraction of each phase in the ZGB cavitation model of the PWK-type pump: oil and vapor mixture (2 phase model).

to be shown in the result presentation as a separate entity which cannot be done in a 2-phase model.

In order to find out the dependence of cavitation on the area of a compensation orifice a different configuration of compensation holes was tested. This time two holes of 1 mm each were used to connect working chambers with the centrally located compensation chamber. That configuration is shown in Fig. 39. An absolute pressure at the area of contact between the compensation orifice and the commutation bushing window reaches 3 MPa, which eliminates a possibility of cavitation occurrence. It turned out that increasing flow cross-section between working and compensation chambers definitely eliminated cavitation in the compensation orifices.

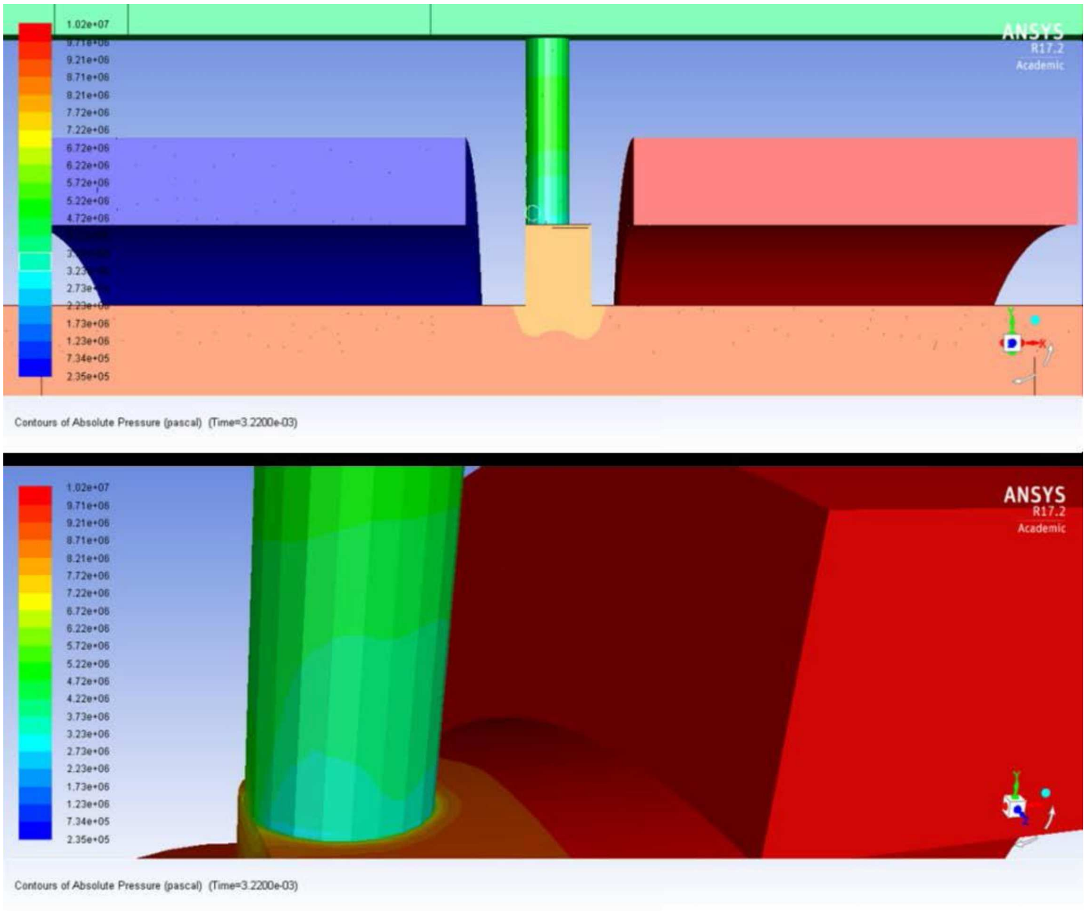

Fig. 38. Contours of absolute pressure in the lower compensation orifice of a 2-hole configuration.

8.2. Influence of the orifice area on mitigating dynamic phenomena

Since the response of the compensation membrane to oil pressure was insufficient to eliminate pressure peaks, the volume flow of oil from the working chamber during its transfer under the bridge had to be increased. Three compensation hole configurations were considered for the pump displacement of 20%:

Configuration 1: with 2 symmetric holes of 1.4 mm diameter (surface area equal to $1.55 \cdot 10^{-6}$ m^2).

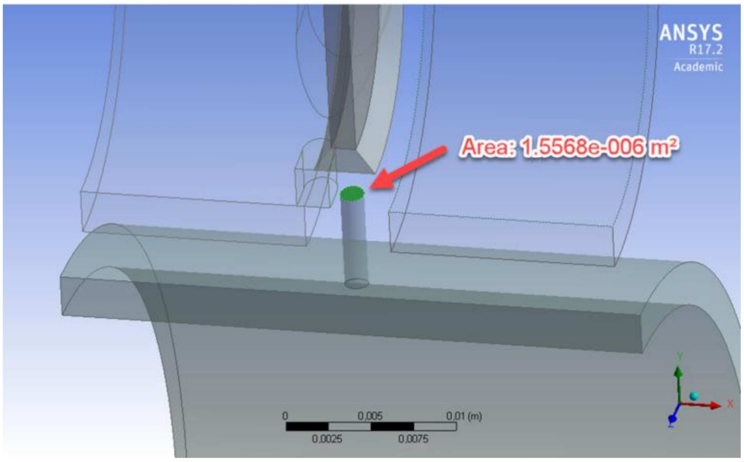

Fig. 39. 2-chamber symmetric model with a compensation hole of 1.4 mm diameter.

Configuration 2: formed by an opening created from connecting those two holes (width equal to 1.4 mm, surface area equal to $3.17 \cdot 10^{-6}$ m^2).

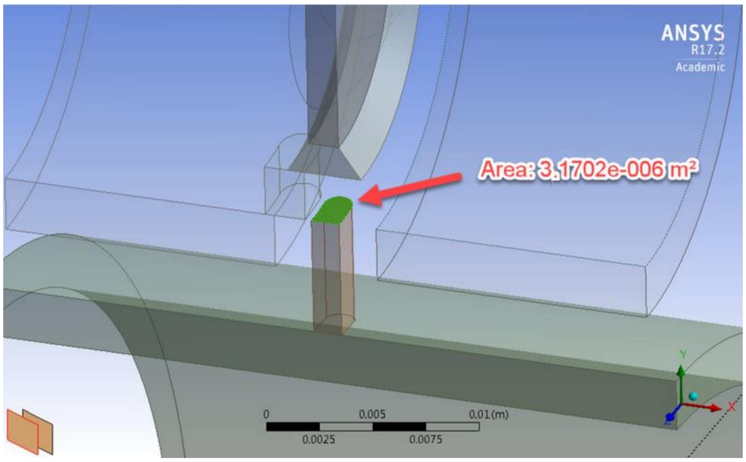

Fig. 40. Compensation opening formed by connecting two relief holes together (original holes are symmetrically distanced from the plane of symmetry).

Configuration 3: formed by an opening overlapping with the window of the commutation bushing (width equal to 2 mm, surface area equal to $5.65 \cdot 10^{-6}$ m^2).

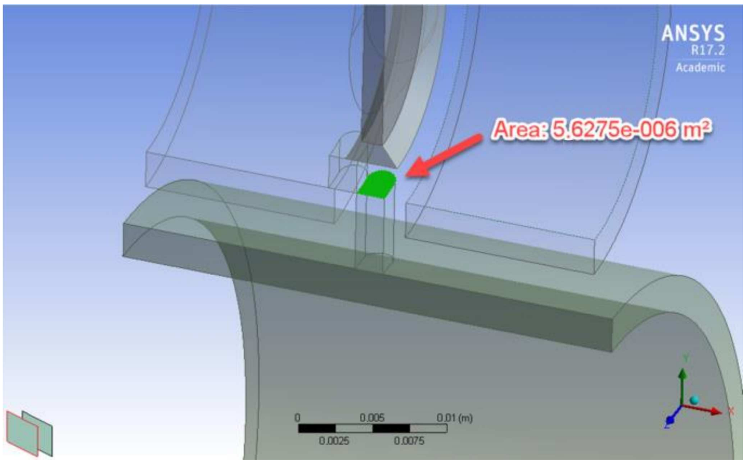

Fig. 41. Compensation opening overlapping with the window in the commutation bushing.

Analysis for configuration 1 was conducted for the displacement of 20% and shaft rotational speed of 1500 rpm. The results are shown in Fig. 42. Figure 43 presents the results of the analysis for configuration 2. A comparison of pressure peaks for configurations 1 and 2 demonstrates a visible decrease of the peak pressure value for configuration 2.

The results for configuration 3 are shown in Fig. 44.

A trend curve connecting peak pressure values for compensation passages of different surface areas is very similar to a plot resulted from experimental tests (see Fig. 45).

Because the analyses presented so far did not include leakages in a pump, which by definition lower the pressure level, a new model which considered the leakage in the helical throttle was developed, since that leakage had the biggest contribution of all pump leakages in the total oil leakage.

The surface area of the hole in the piston was corresponding to the cross sectional area of the oil passage in the throttle (0.8×0.5 mm). Calculations were carried out for 3 configurations

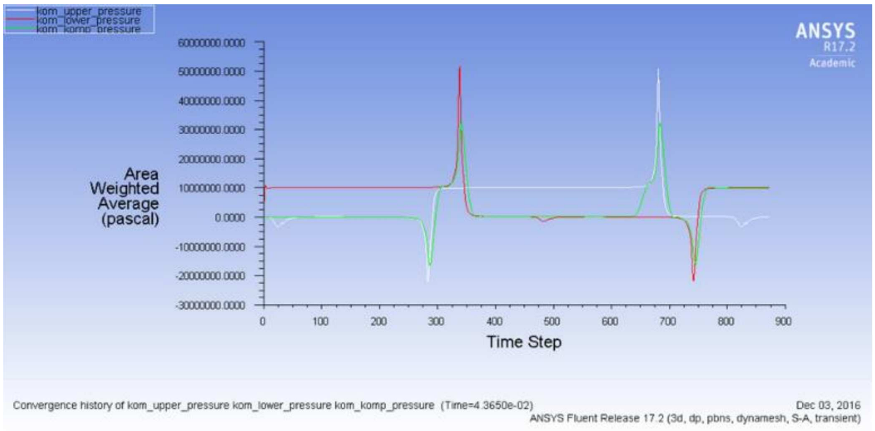

Fig. 42. Distribution of pressure for configuration 1 (a compensation hole of 1.4 mm diameter, displacement 20%, 1500 rpm, temperature 56°C). The model did not consider leakages in the pump.

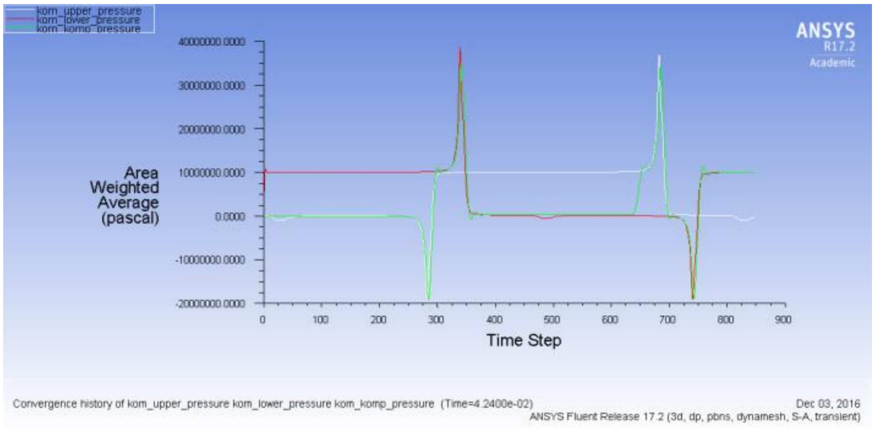

Fig. 43. Distribution of pressure for configuration 2 (surface area equal to $3.17e^{-6}$ m^2, displacement 20%, 1500 rpm, temperature 56°C). No leakage was considered.

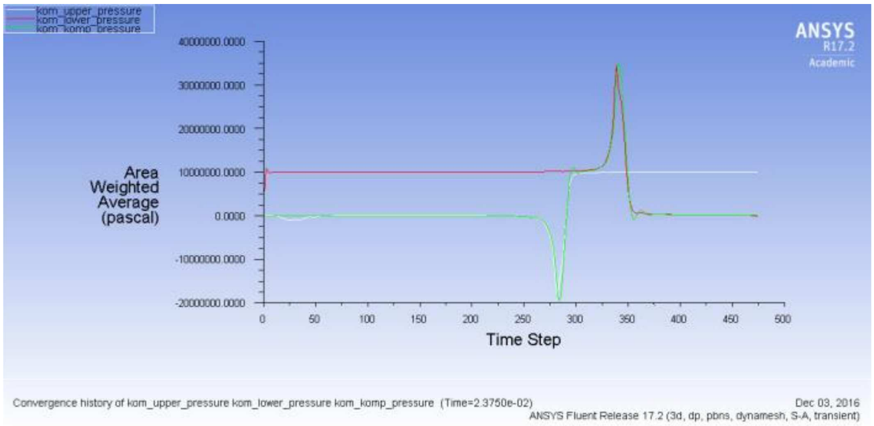

Fig. 44. The pressure distribution for configuration 3 (surface area equal to $5.65 \cdot 10^{-6}$ m^2, displacement 20%, 1500 rpm, temperature 56°C). No leakage was considered.

of the compensation orifices at 20% displacement and 1500 rpm. Figure 47 shows the pressure plot derived from the analysis of the model for configuration 3 which considered pump leakage. Such modification decreased the pressure peak by 8 MPa for that configuration.

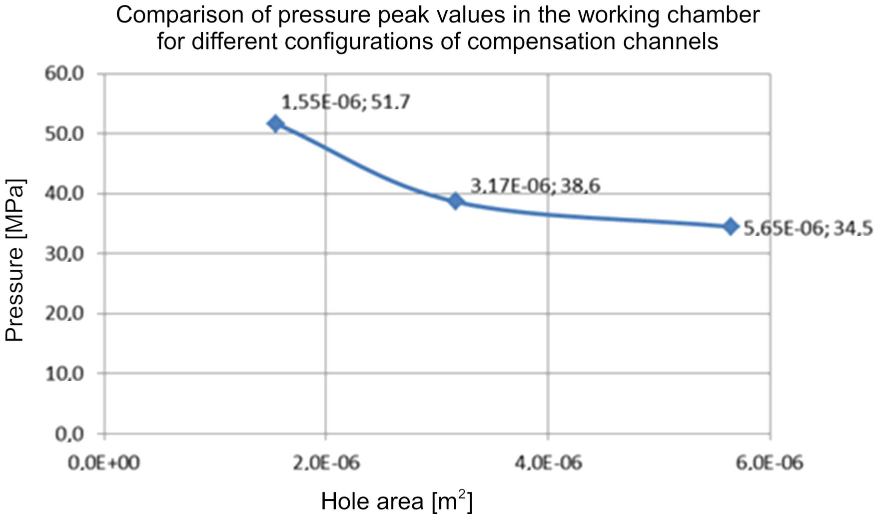

Fig. 45. Pressure peak values for different pressure relief hole configurations – displacement 20%, 1500 rpm, temperature 56°C). The first label on the plot denotes the surface area the second is the value of pressure.

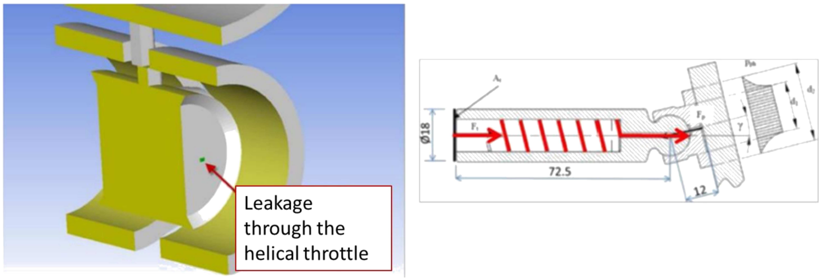

Fig. 46. Leakage through the helical throttle placed in a piston was considered in the simulation model of PWK-type pump.

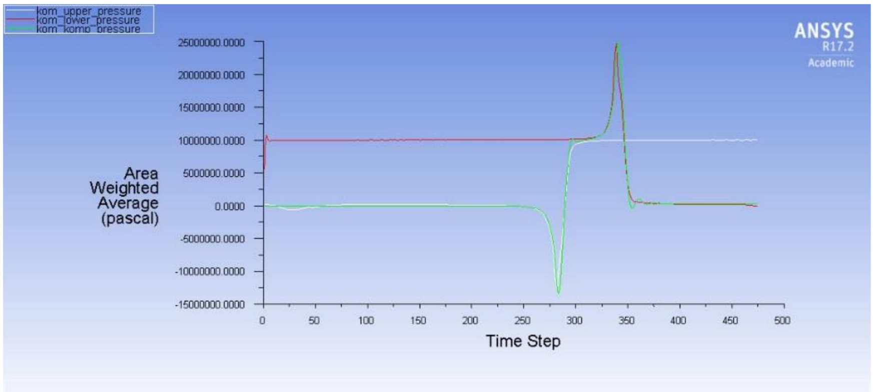

Fig. 47. Pressure plot for configuration 3 (surface area of the relief hole is equal to $5.65 \cdot 10^{-6}$ m^2, displacement 20%, 1500 rpm, temperature 56°C). Leakages in the pump were considered.

Figure 48 presents a comparison of results of a simulation done for 20% displacement and the pumping pressure of 10 MPa with an experiment [10].

The right portion of Fig. 48 shows a red curve which corresponds to a pressure peak with leakage in the pump not taken into account. The blue curve includes the correction for a leakage. The difference between a simulation (5.6 MPa) with the result measured during an experiment (6 MPa) shows a good agreement.

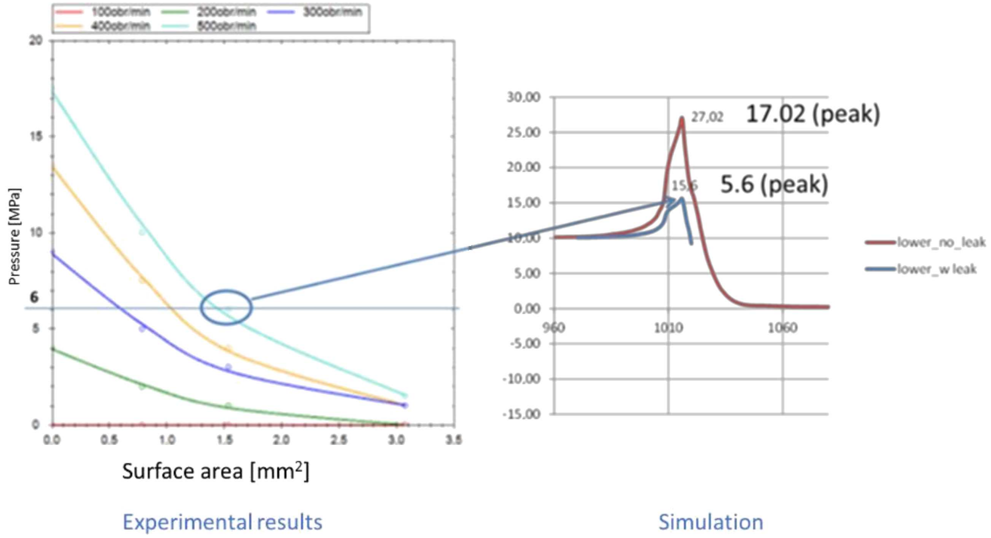

Fig. 48. Comparison of simulation results with experiment [10]. A relief hole of 1.4 mm diameter, 20% displacement, 500 rpm.

Reducing rotational speed decreased the pressure peak in the working chamber to 2.6 MPa (see Fig. 49). That simulation value compared to the experimental result of 3 MPa is acceptable.

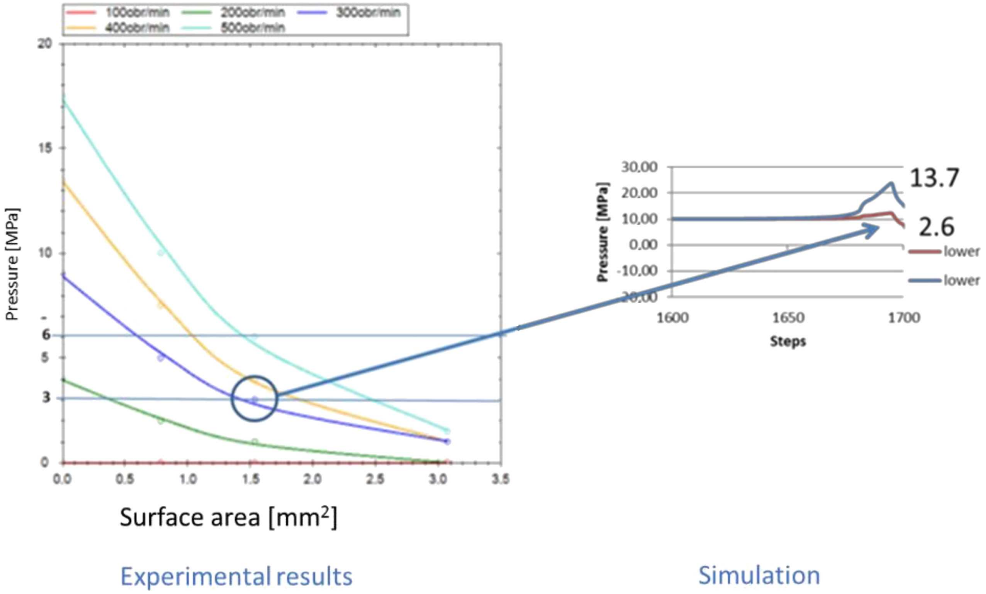

Fig. 49. Comparison of results between a simulation and an experiment for a hole of 1.4 mm diameter, 300 rpm and displacement 20% [10]. Red curve with 2.6 MPa peak considers a leakage.

The proposed method of reducing pressure peaks in a working chamber by evacuating excessive oil through the increased pressure relief passages seems to be a viable mitigation approach and the results obtained both in calculations and experiments corroborate that solution.

9. CONCLUSIONS

Dynamic phenomena occurring in a design of a multi-piston axial hydraulic pump equipped with a cam-driven commutation unit present a challenge. Their elimination is very often difficult owing to a complex nature of such events. Simulation by numerical methods provides a useful way to help solving such difficult problems.

Virtual prototyping allows the designers cut expenses and time in arriving at the optimal design, frequently allowing operations that would not be doable in real life owing to the susceptibility of components to failure stemming from excessive loads or the transient character of those rapidly changing phenomena.

The PWK-type multi-piston axial hydraulic pump could be considered a breakthrough in the design of hydraulic machinery. However, the pump displacement variability posed serious problems connected with pressure peaks. A systematic way to solve those problems was implemented and a viable solution was presented, proving that an implementation of PWK-type design is possible.

REFERENCES

[1] *ANSYS Fluent Theory Guide, Release 15.0.* November, 2013.

[2] A. Osiecki. *Hydrostatic Machine Drive* [in Polish: *Hydrostatyczny Napęd Maszyn*]. Wydawnictwa Naukowo-Techniczne, Warszawa, Poland, 2004.

[3] A. Osiecki. *Drive and Hydraulic Control of Machines – Theory, Calculation and Systems* [in Polish: *Napęd i Sterowanie Hydrauliczne Maszyn – Teoria, obliczanie i układy*]. Politechnika Gdanska, Gdańsk, Poland, 1995.

[4] A. Osiecki. *Piston Pump with a Constant Working Volume.* International Patent PL191366 (A1. 07 31), 1978.

[5] A. Osiecki, L. Osiecki. *Hydrostatic Axial Piston Machine.* International Patent EP0742870A1. 04 14, 1999.

[6] L. Osiecki. *Mechanisms of the Timing of Hydraulic Axial Multi-Piston Machines* [in Polish: *Mechanizmy Rozrządu Hydraulicznych Maszyn Wielotłoczkowych Osiowych*]. Politechnika Gdanska, Gdańsk, 2006.

[7] L. Osiecki. *Multipiston Axial Hydrostatic Machine.* International Patent PL387933A1. 08 11, 2010.

[8] L. Osiecki. *Multipiston Axial Hydrostatic Machine.* International Patent PL215652B1. 01 31, 2014.

[9] L. Osiecki, P. Patrosz, T. Zawistowski, B. Landvogt, J. Piechna, B. Zylinski. Compensation of pressure peaks in PWK-type hydraulic pumps. *Key Engineering Materials*, **490**: 33–44, 2011.

[10] P. Patrosz. *Compensation of pressure peaks in a variable displacement piston pump with cam driven commutation* [in Polish: *Kompensacja skoków ciśnienia w pompie tłoczkowej o zmiennej wydajności z rozrządem krzywkowym*]. D.Sc. Thesis, 2017.

[11] T. Zawistowski, M. Kleiber. Gap flow simulation methods in high pressure variable displacement piston pumps. *Archives of Computational Methods in Engineering*, **24**: 519–542, 2017.

[12] S.K. Maity, R. Kawalla. Ultrahigh Strength Steel: Development of Mechanical Properties Through Controlled Cooling, http://cdn.intechweb.org/.